Fifteen new T dwarfs discovered in the UKIDSS Large Area Survey

D. J. Pinfield[1]⋆, B. Burningham[1], M. Tamura[2], S. K. Leggett[3], N. Lodieu[4],
P. W. Lucas[1], D.J. Mortlock[5], S. J. Warren[5], D. Homeier[6], M. Ishi[7], N. R. Deacon[8],
R. G. McMahon[9], P. C. Hewett[9], M. R. Zapatero Osorio[4], E. L. Martin[4],
H. R. A. Jones[1], B.P. Venemans[9], A. Day-Jones[1], P. D. Dobbie[10], S. L. Folkes[1],
S. Dye[11], F. Allard[12], I. Baraffe[13], D. Barrado y Navascués[14], S. L. Casewell[15],
K. Chiu[16], G. Chabrier[13], F. Clarke[17], S. T. Hodgkin[9], A. Magazzù[18],
M. J. McCaughrean[16], E. Moraux[19], T. Nakajima[2], Y. Pavlenko[20], C. G. Tinney[21]

[1] Centre for Astrophysics Research, Science and Technology Research Institute, University of Hertfordshire, Hatfield AL10 9AB
[2] National Astronomical Observatory, Mitaka, Tokyo 181-8588
[3] Gemini Observatory, 670 N. A'ohoku Place, Hilo, HI 96720, USA
[4] Instituto de Astrofísica de Canarias, 38200 La Laguna, Spain
[5] Astrophysics Group, Imperial College London, Blackett Laboratory, Prince Consort Road, London SW7 2AZ
[6] Institut fur Astrophysik, Georg-August-Universitat, Friedrich-Hund-Platz 1, 37077 Gottingen, Germany
[7] Subaru Telescope, 650 North A'ohoku Place, Hilo, Hi 96720, USA
[8] Department of Astrophysics, Faculty of Science, Radboud University Nijmegen, PO Box 9010, 6500 GL Nijmegen, The Netherlands
[9] Institute of Astronomy, Madingley Road, Cambridge CB3 0HA, UK
[10] Anglo-Australian Observatory, P.O. Box 296, Epping 1710, Australia
[11] Cardif University, School of Physics & Astronomy, Queens Buildings, The Parade, Cardif, CF24 3AA, U.K.
[12] Centre de Recherche Astrophysique de Lyon, UMR5574, CNRS, Universite de Lyon, Ecole Normale Superieure, 46 Allee d'Italie, F-69364 Lyon Cedex 07, France
[13] C.R.A.L. (UMR 5574 CNRS), Ecole Normale Superieure, 69364 Lyon Cedex 07, France
[14] Laboratorio de Astrofísica Espacial y Física Fundamental, INTA, P.O. Box 50727, E–2808 Madrid, Spain
[15] Department of Physics and Astronomy, University of Leicester, University Road, Leicester LE1 7RH, UK
[16] School of Physics, University of Exeter, Stocker Road, Exeter EX4 4QL, Devon, UK
[17] European Southern Observatory, Alonso de Cordova 3107, Casilla 19001 Santiago 19, Chile

2 June 2008

ABSTRACT
We present the discovery of fifteen new T2.5-T7.5 dwarfs (with estimated distances between ∼24–93pc), identified in the first three main data releases of the UKIRT Infrared Deep Sky Survey. This brings the total number of T dwarfs discovered in the Large Area Survey (to date) to 28. These discoveries are confirmed by near infrared spectroscopy, from which we derive spectral types on the unified scheme of Burgasser et al. (2006). Seven of the new T dwarfs have spectral types of T2.5-T4.5, five have spectral types of T5-T5.5, one is a T6.5p, and two are T7-7.5. We assess spectral morphology and colours to identify T dwarfs in our sample that may have non-typical physical properties (by comparison to solar neighbourhood populations), and find that one of these new T dwarfs may be metal poor, three may have low surface gravity, and one may have high surface gravity. The colours of the full sample of LAS T dwarfs show a possible trend to bluer $Y-J$ with decreasing effective temperature, and some interesting colour changes in $J-H$ and $z-J$ (deserving further investigation) beyond T8. The LAS T dwarf sample from the first and second main data releases show good evidence for a consistent level of completion to J=19. By accounting for the main sources of incompleteness (selection, follow-up and spatial) as well as the effects of unresolved binarity and Malmquist bias, we estimate that there are 17±4 ⩾T4 dwarfs in the $J \leqslant 19$ volume of the LAS second data release. Comparing this to theoretical predictions is most consistent with a sub-stellar mass function exponent α between -1.0 and 0. This is consistent with the latest 2MASS/SDSS constraint (which is based on lower number statistics), and is significantly lower than the $\alpha \sim 1.0$ suggested by L dwarf field populations, possibly a result of the lower mass range probed by the T dwarf class.

1 INTRODUCTION

The advent of the large scale Sloan Digital Sky Survey (SDSS; York et al. 2000), the 2-Micron All Sky Survey (2MASS; Skrutskie et al. 2006) and Deep Near Infrared Survey of the Southern Sky (DENIS; Epchtein et al. 1997) were the main factors that led to the identification and study of the two spectral classes beyond M; the L dwarfs (with effective temperature T_{eff} ~2300-1450K; Golimowski et al. 2004) have dusty atmospheres and very red near infrared colours, while the even cooler T dwarfs (T_{eff} <1450K) have clear atmospheres (from which the dust has settled), and their blue infrared spectra are dominated by strong CH_4 and H_2O absorption bands. The spectral typing scheme of Kirkpatrick et al. (1999) established the first properly classified L dwarf population via 2MASS discoveries. The first T dwarf was discovered as a close companion to the early M dwarf GL229 (Nakajima et al. 1995), and the first L dwarf as a companion to the white dwarf GD 165 (Becklin & Zuckerman 1988; Kirkpatrick et al. 1993). However, the subsequent growth of the known T (and L) dwarf populations (>500 L dwarfs and >100 T dwarfs are known at time of writing; Kirkpatrick 2005) has been predominantly achieved via searches of the SDSS (e.g. Leggett et al. 2000; Geballe et al. 2002; Knapp et al. 2004; Chiu et al. 2006) and 2MASS (e.g. Kirkpatrick et al. 2000; Cruz et al. 2007; Burgasser et al. 2002; 2004; Tinney et al. 2005; Looper Kirkpatrick & Burgasser 2007) databases.

The coolest T_{eff} probed by SDSS and 2MASS are currently defined by the eight T7.5-8 dwarfs (as typed by the Burgasser et al. (2006b; B06) scheme) discovered in these surveys. These objects have T_{eff} in the range 725-950K (Geballe et al. 2001; Saumon et al. 2006; 2007; Leggett et al. 2007; Burgasser, Burrows & Kirkpatrick 2006). At lower T_{eff} it is possible that a new spectral class (pre-emptively called Y, following Kirkpatrick et al. (1999)) may be necessary, if for example, spectral changes occur such as the strengthening of ammonia absorption, and/or the condensation of atmospheric water clouds (Burrows, Sudarsky & Lunine (2003)). L and T dwarfs already encompass the temperature scale of transiting "hot Jupiters" (e.g. Knutson et al. 2007), and populating the even cooler T_{eff} regime will allow us to study and understand atmospheres whose T_{eff} is similar to cooler extra-solar giant planets populations.

The current complement of known L and T dwarfs allows some constraints to be placed on the substellar mass function (e.g. Chabrier 2003 and references therein; Allen et al. 2005; Metchev et al. 2007). However, if the brown dwarf mass function is to be accurately constrained, a significantly larger number of late T dwarfs will be extremely beneficial, since the T_{eff} distribution of T dwarfs in the <950K range is particularly sensitive to mass function variations (e.g. fig 5 of Burgasser 2004). Also, accurate constraints on the brown dwarf birth rate (i.e. their formation history) need the improved statistics that come with larger numbers of both L and T dwarfs.

The UKIRT (UK Infrared Telescope) Infrared Deep Sky Survey (UKIDSS; Lawrence et al. 2007) is a new infrared survey being conducted with the UKIRT Wide Field Camera (WFCAM; Casali et al. 2007). UKIDSS is a set of five sub-surveys, with three wide field surveys – the Large Area Survey (LAS), the Galactic Cluster Survey (GCS) and the Galactic Plane Survey (GPS) – and two very deep surveys – the Deep Extra-galactic Survey (DXS) and the Ultra-Deep Survey (UDS). The LAS is the largest of the wide-field surveys, and will cover 4000 sq degs of sky in four filter bands, going several magnitudes deeper than 2MASS. UKIDSS began in May 2005, and at the time of writing there have been four ESO (European Southern Observatory)-wide releases, including an Early Data Release (EDR) in February 2006 (Dye et al. 2006), and three subsequent main data releases: Data Release 1 (DR1) in 2006 July covering 190 sq degs (Warren et al. 2007b), Data Release 2 (DR2) in 2007 March covering 280 sq degs (including DR1; Warren et al. 2007c), and Data Release 3 (DR3) in 2007 December, covering 900 sq degs (including DR1 and DR2).

These data are providing un-paralleled sensitivity to L and T dwarf populations, and our collaboration has begun a variety of UKIDSS-based searches for these objects. Here we focus on our search for late T dwarfs and potentially new record breaking low-T_{eff} objects. Previous LAS T dwarfs have been presented by Kendall et al. (2007), Lodieu et al. (2007), Warren et al. (2007a) and Chiu et al. (2008), who have discovered a total of 13 spectroscopically confirmed LAS T dwarfs from the EDR and DR1. This included the first T8.5 dwarf ULAS J0034-0052 (Warren et al. 2007a).

Here we report the discovery of 15 new LAS T dwarfs discovered in DR1, DR2 and some of DR3. Section 2 summarises our selection criteria for identifying candidate T dwarfs as well as possible 400-700K objects. Section 3 describes the follow-up photometry we have obtained to identify spurious objects amongst these candidates, and Section 4 presents our spectroscopic follow-up and confirmation of the 15 new T dwarfs. Section 5 discusses the spectral morphology and colour of the new T dwarfs and how these could relate to their physical properties, and Section 6 presents updated constraints on the size of the LAS T dwarf population, compared to theoretical predictions. Section 7 discusses some future work and gives our conclusions.

2 IDENTIFYING T DWARF CANDIDATES

In this section we describe our photometric search for T dwarfs and cooler 700–400K objects (potential Y dwarfs). We will focus this description on our searches of DR1 and DR2, since our follow-up of candidates from these data releases has a reasonably well constrained level of completion, and issues such as contamination amongst the candidates will be addressed more usefully. However, the process of T dwarf identification is ongoing with DR3, using these same techniques. Note also that some DR1 results have previously been published (Kendall et al. 2007; Lodieu et al. 2007; Warren et al. 2007), but for clarity we here describe our search of DR1 and DR2 as a whole.

We base our search on the current knowledge of $izJHK$ properties of known objects previously discovered in 2MASS and SDSS, as well as on colour trends suggested by the latest theoretical atmosphere models for T_{eff} ranges below those that are well probed by previous surveys. We also make use of LAS magnitudes measured using the new Y filter (0.97–1.07μm), which was specifically designed and installed in WFCAM to ease the selection and separation of high-

redshift quasars and cool brown dwarfs (Warren & Hewett 2002).

2MASS T dwarfs have neutral to blue near infrared colours with decreasing $T_{\rm eff}$ (Burgasser et al. 2002), and a fairly uniform $Y - J \sim 1$ (from synthesized colours; Hewett et al. 2006). Late T dwarfs are clearly well separated from redder L dwarfs by their $J - H$ colour (although there is some $J - H$ colour overlap for early T dwarfs), and from earlier objects by, in general, both $J - H$ and $Y - J$ colour (see Figure 1). The model predictions suggest that the near infrared colours will remain blue ($J - H < 0.0, J - K < 0.0$) for 400-700K. However, while the models uniformly predict that the 400-700K dwarf colour sequence should form an extension of the known T dwarfs, they differ somewhat on their predicted $Y - J$ colour trends. The cloud-free Cond models (Allard et al. 2001; Baraffe et al. 2003), the more recent Settl models (Allard et al., in preparation) and the Marley et al. (2002) models all suggest a blue $Y - J$ colour trend, while the Burrows et al. (2003) and Tsuji, Nakajima & Yanagisawa (2004) models suggest a red $Y - J$ colour trend for this $T_{\rm eff}$ regime.

In addition, known T dwarfs from SDSS have very red ($i - z \geqslant 2.2$) optical colours, and extremely red optical-to-infrared colours ($z - J \geqslant 2.5$; note that here and hereafter i and z are AB magnitudes whereas J is on the Vega system), the latter being a particularly good indicator of $T_{\rm eff}$ for early-mid T dwarfs (Knapp et al. 2004). The model predictions suggest that these extreme optical and optical-to-infrared colours should continue to be strong indicators of low-$T_{\rm eff}$ in the 400-700K regime. A combination of $YJHK$ photometry from the LAS and deep optical constraints from SDSS thus offer an extremely powerful tool to identify samples of mid-late T dwarfs and even cooler objects to photometric depths several magnitudes deeper than previous wide-field surveys.

2.1 Initial sample selection

Our search methodology was to mine (via the WFCAM Science Archive; Hambly et al. 2007) the LAS for objects with $YJHK$ photometry consistent with known T dwarfs or with the expected colours of 400-700K objects using the models as a guide, and then cross-match with SDSS (where possible) obtain optical-to-infrared constraints. Here we describe three sets of search criteria that probe to different depths in DR1 and DR2, requiring coverage in all four $YJHK$ bands, but relying on source detection in different numbers of bands.

Our first search method required $YJHK$ detection with $Y - J \geqslant 0.8$ and $J - H \leqslant 0.4$ (to separate T dwarfs from L dwarfs). This method is limited by the $K-$band for mid-late T dwarfs, does not probe the full range of $Y - J$ colour for potential 400-700K objects, and is thus better at finding brighter early T dwarfs which can have redder $H - K$ colour. We also cross-matched objects with SDSS, requiring a detection with $i - z \geqslant 2.2$ and $z - J \geqslant 2.5$. While we also performed searches requiring optical non-detection, we postpone analysis of these candidates to a future publication, and here present the one new object identified with a SDSS detection; ULAS J115759.04+092200.7 (see Table 1).

Our second search method required YJH LAS detection and a K non-detection, and probed the colour space

shown in Figure 1, including objects with $J - H \leqslant 0.1$ and $Y - J \geqslant 0.5$. This search is H-band limited for objects with blue $J - H$, but fully probes the range of 400-700K colour space suggested by the models. Candidates were cross-matched with SDSS and rejected if found to be optical detections with either $i - z < 2.2$ or $z - J < 2.5$, or found to have no SDSS coverage. This search produced a sample of 33 candidates.

Our third search method required YJ LAS detection and HK non-detection, with $Y - J \geqslant 0.5$. For objects with blue $J - H$ this search is J-band or Y-band limited for $Y - J \leqslant 0.8$ and $Y - J \geqslant 0.8$ respectively, and probes to a greater depth than method 2. SDSS cross-matching constraints were imposed as before, and resulted in a sample of 45 candidates.

In addition we used our second search method to search the LAS sky outside the SDSS DR6 footprint, substituting our SDSS optical constraints for shallower Schmidt plate I-band coverage from the SuperCOSMOS sky survey. This search identified 24 candidates.

Figure 1 shows the $J - H$, $Y - J$ two-colour diagram and the J against $J - H$ colour magnitude diagram for the T dwarf and $T_{\rm eff}$=700–400K candidates from DR1 and DR2. Candidates are either crosses (where $Y-$, $J-$ and $H-$band detections were available) or arrows (where H was a non detection). A sample of L dwarf candidates (plus signs; LAS $Y - J > 0.9$, $J - H > 0.5$, $J - K > 1.2$, and SDSS $z < 20.8$) is also shown for comparison (some spectroscopically confirmed L dwarfs from this sample will be reported in a separate paper), as is a sample of typical brighter sources from the LAS (points). These brighter sources were selected from a one degree radius area of DR2 sky at high Galactic latitude, and have YJHK magnitude uncertainties less than 0.03 magnitudes and a Sloan counterpart. The L dwarf candidates are being followed up, but we will not discuss them further here, showing them purely for comparison. Our YJH selection box ($Y - J > 0.5$, $J - H < 0.1$) is indicated with a dashed line, and contains over-plotted boxes (dotted and dot-dashed lines) that illustrate the range of model predictions for $T_{\rm eff}$=700–400K (see figure caption).

Candidates from our DR1-3 searches that have been confirmed as T dwarfs via spectroscopy (see Section 4) are shown in Table 1, which summarises the database release in which they were first found, as well as the bands that were used to make the searches. All of our new T dwarfs are in SDSS DR6 sky, although two previously confirmed candidates (Lodieu et al. 2007) are outside the SDSS DR6 footprint. Figure 2 presents finding charts for the 15 new T dwarfs.

3 FOLLOW-UP PHOTOMETRY

Photometric contamination amongst our candidates has several causes. In general, photometry near the survey limits will have significant uncertainties due to low signal-to-noise ratio and/or survey image defects (see Dye et al. 2006), and in certain circumstances normal stars can have their colours scattered to the blue. Scattered late M dwarfs with $J > 18$ will not always be ruled out via SDSS non detection if their $i - J = 3$-4 (the 5-σ SDSS i-band limit is $\sim$22). Also, if LAS images in different bands are measured on different nights, variable sources can yield extremely blue survey colours, and
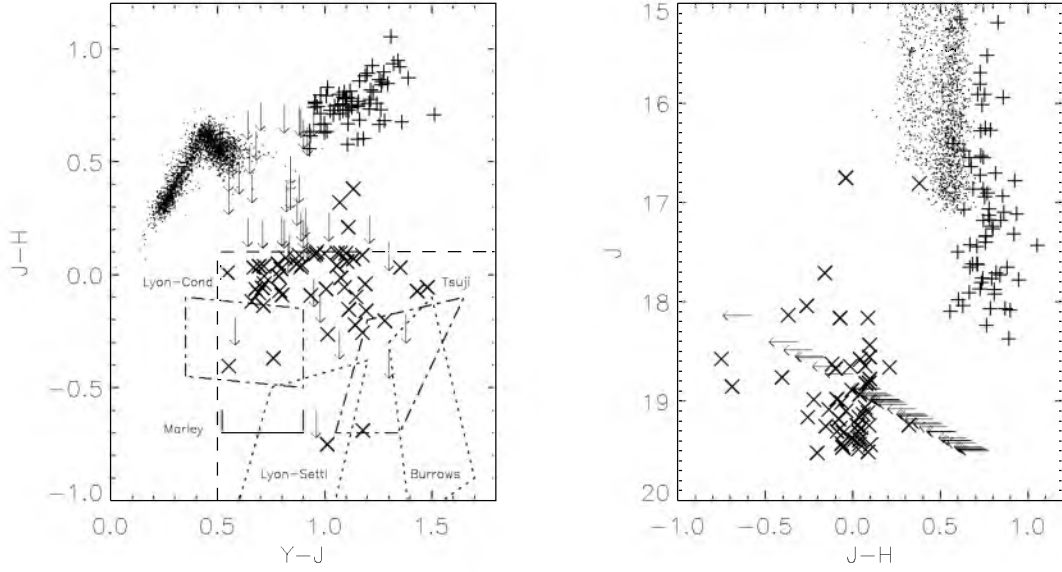
Figure 1. A $J - H$ against $Y - J$ two-colour diagram and a J against $J - H$ colour magnitude diagram showing candidate late T and Y dwarfs from DR1 and DR2. $YJH(K)$ candidates are shown as crosses, and YJ candidates as upper limit arrows. An illustrative L dwarf candidate sample is shown by plus signs. Our YJH candidate selection box is shown with a dotted line, and contains theoretical model predicted colours for T_{eff}=400-700K dwarfs from: the cloud-free Lyon-Cond models (Allard et al. 2001; Baraffe et al. 2003); the more recent Lyon-Settl models (Allard et al., in preparation); the AMES models (e.g. Marley et al. 2002; Saumon et al. 2003); the Tucson models (e.g. Sharp 2000; Burrows Sudarsky & Hubeny 2006); and the Tsuji models (Tsuji Nakajima & Yanagisawa 2004).

Table 1. Newly discovered UKIDSS T dwarfs. The table lists the coordinates, the UKIDSS LAS database release in which objects were found, and the bands that were used to make the searches in which the objects were identified. All objects have SDSS coverage, although only one is detected in SDSS. The table contains the newly confirmed T dwarfs as well as (at the bottom) three that we rule out with spectroscopy.

Name[a]	Database	NIR band detections	SDSS band detections
ULAS J022200.43 − 002410.5	DR1	YJH	-
ULAS J082327.46 + 002424.4	DR3	$YJHK$	-
ULAS J083756.19 − 004156.0	DR1	YJH	-
ULAS J085910.69 + 101017.1	DR3	$YJHK$	-
ULAS J093829.28 − 001112.6	DR3	YJH	-
ULAS J093951.04 + 001653.6	DR3	YJH	-
ULAS J095829.86 − 003932.0	DR1	YJ	-
ULAS J115038.79 + 094942.9	DR2	YJH	-
ULAS J115759.04 + 092200.7	DR2	$YJHK$	i, z
ULAS J130303.54 + 001627.7	DR1	YJ	-
ULAS J131508.42 + 082627.4	DR2	YJH	-
ULAS J150135.33 + 082215.2	DR2	YJ	-
ULAS J150547.89 + 070316.6	DR2	YJ	-
ULAS J154427.34 + 081926.6	DR2	YJ	-
ULAS J154701.84 + 005320.3	DR2	YJH	-
ULAS J003925.90 + 000257.7	DR1	YJH	-
ULAS J130150.35 + 002314.8[b]	EDR	YJH	-
ULAS J224355.03 − 004618.5	DR1	YJH	-

[a] Here the source names include full coordinates. In subsequent tables/figures the source names are truncated.

[b] First reported as a T dwarf candidate by Kendall et al. (2007).

Figure 2. Finding charts for the 15 new T dwarfs discovered in the UKIDSS LAS and presented in this paper. Charts are $J-$band images of generally two arcmin on a side (unless constrained by the edge of a UKIDSS frame) with north up and east left. Indicated spectral types are infrared types derived here.

fast moving solar system objects can appear as detections at Y and J while being undetected (at that position) in H and K (e.g. LAS YJ observations are sometimes taken on different nights to the HK observations of the same region). Galaxies can also have unusual colours that could contaminate our selections.

We used deeper follow-up J- and H-band photometry to identify such contamination, re-measuring the $J - H$ colour at a higher signal-to-noise ratio and identifying any extended sources. We also obtained deeper Y-, K- and z-band photometry of a number of our best candidates to provide a more complete range of colours with which to assess candidate properties. We used a variety of facilities to obtain our infrared and optical follow-up photometry, and we summarise these measurements for confirmed T dwarfs in Table 2. In general this table presents photometry for the newly discovered T dwarfs, but also includes additional z-band measurements for two previously reported LAS T dwarfs from Lodieu et al. (2007).

3.1   Near infrared photometry

Near infrared follow-up photometry was obtained with three facilities. We used WFCAM and the UKIRT Fast-Track Imager (UFTI; Roche et al. 2003) on UKIRT, both of which employ the Mauna Kea Observatories (MKO) J, H and K filters (Tokunaga, Simons & Vacca 2002), as well as the UKIDSS Y filter (Hewett et al. 2006). We also used the Long-slit Infrared Imaging Spectrograph (LIRIS; Manchado et al. (1998)) instrument on the William Herschel Telescope on La Palma in the Canaries, which uses MKO J and H filters, a K_s filter, and a z_{Liris} filter that is quite similar (although slightly narrower band; 1.00–1.07μm) to WFCAM Y. It also has a narrow band methane filter (CH_4l; 1.64–1.74μm) that we used to measure one of the new T dwarfs presented here.

Observations comprised a series of jittered (by a few arcsec) image sets, as well as (for WFCAM observations) subsets of micro-stepped images that improve the pixel sampling during processing. Individual exposure times ranged from 10s to 216s, and a summary of the different combinations of micro-step, jitter, repeat, individual exposure time and total exposure times, is given in Table 2. All observations were made during photometric conditions with good to reasonable seeing (0.6-0.8 arcsec). The data was dark-subtracted, flat fielded and mosaiced using standard ORAC-DR routines for the UFTI data, LIRIS-DR routines for the LIRIS data, and the Cambridge Astronomical Survey Unit's Vista data-flow system (Irwin et al. 2004) for the WFCAM observations. Photometry was then performed using typical aperture sizes of ~2-arcsec diameter.

The UFTI observations were calibrated using UKIRT Faint Standards, so the photometric system was thus identical to the WFCAM system (Leggett et al. 2006). The WFCAM magnitudes were obtained via flat-file access from the WFCAM Science Archive. The LIRIS J-, H- and K_s-band observations were calibrated using 2MASS stars as secondary standards where J and H magnitudes were converted onto the MKO system via transforms from Warren et al. (2007c). 2MASS uses the same K_s filter as LIRIS, so no 2MASS standard K conversion was necessary when determining LIRIS K_s magnitudes for our candidates. LIRIS

CH_4l photometry was calibrated by assuming that the average $H - CH_4l$ colours of 2MASS secondary calibrators was zero (see also Kendall et al. 2007). The LIRIS z observations were calibrated using observations of A0 stars at similar airmass to our target observations, where $(z - J)_{A0}$=0 was assumed.

In order for the T dwarf photometry to be in the same photometric system, we converted our LIRIS z and K_s measurements to MKO Y and K. Transforms were determined via synthetic colours derived from measured T dwarf spectra multiplied by the appropriate atmospheric and filter transmission profiles, following the methods of Hewett et al. (2006). We derived $Y - z_{Liris}$ and $K - K_s$(LIRIS) colours for the standard T dwarfs from B06 as well as for the T dwarfs used in Hewett et al. (2006), excepting objects that have been shown to be unresolved binaries (Liu et al. 2006; Burgasser et al. 2006a). The $Y - z_{Liris}$ colours show no trend with spectral type, and a conversion of $Y=z_{Liris}+(0.015\pm0.011)$ was determined. The $K - K_s$(WHT) colours display a tightly defined sequence monotonically increasing with spectral type such that $K=K_s$(WHT)$+(0.032\times$ST)-0.01, with a scatter of 0.01 magnitudes (where ST=1, 2, 3... for T1, T2, T3...).

3.2   Optical photometry

Optical $z-$band follow-up photometry was obtained with the European Southern Observatory (ESO) Multi-Mode Instrument (EMMI) on the New Technology Telescope on La Silla, Chile. A Bessel $z-$band filter was used (EMMI#611; z_{EMMI}) which has a short wavelength cut-off of 825μm and is an open-ended filter, where the CCD sensitivity provides the longer wavelength cut-off. The conditions were clear, with seeing of ~1 arcsec. The EMMI data were reduced using standard IRAF routines including a bias and flat-field correction, as well as the removal of fringing effects. Multiple images of the same sky areas were then aligned and co-added. Aperture photometry was measured using ~1.5 arcsec apertures, and we calibrated this photometry using Sloan sources (York et al. 2000) contained in the images as secondary standards. This method allowed us to derive image zero points with a typical accuracy of ±0.05 magnitudes. We transformed the Sloan AB photometry of our secondary standards into the EMMI system using the transformation of Warren et al. (2007a). We then derived z_{EMMI} (AB) photometry for the targets, and then transformed these into the Sloan AB magnitudes assuming that z(AB)=z_{EMMI}(AB)+0.2 (Warren et al. 2007a). Our optical $z-$band photometry is thus all in the Sloan AB system.

3.3   Photometric results

We have been able to reject 61 of our 103 DR1 and DR2 candidates via follow-up photometry, since the $J - H$ colours were found to be $\geqslant0.4$, and the candidates thus likely M or L dwarfs. A total of 23 DR1 and DR2 T dwarfs have been confirmed amongst the remaining candidates, including 11 of the 15 new T dwarfs reported here (four are from DR3), and 12 previously reported: one by Geballe et al. (2002), one by Kendall et al. (2007), one by Warren et al. (2007a), eight by Lodieu et al (2007), and one by Chiu et al. (2007). Near

Table 2. Follow-up near infrared and optical photometric observations

Name	Instrument & telescope	Filter	UT date	t_{int} (m=micro-steps, j=jitters, r=repeats)[a]
ULAS J0222 − 0024	UFTI/UKIRT	J	2007 Jul 24	300s (j=5, t_{exp}=60s)
		H		1800s (j=5, r=6, t_{exp}=60s)
		K	2007 Jul 28	1590s (j=5, r=6, t_{exp}=53s)
		Y		600s (j=5, t_{exp}=120s)
	EMMI/NTT	z_{EMMI}	2007 Nov 17	2400s (r=4, t_{exp}=600s)
ULAS J0823 + 0024	EMMI/NTT	z_{EMMI}	2007 Nov 17	900s (r=2, t_{exp}=450s)
ULAS J0837 − 0041	WFCAM/UKIRT	J	2007 May 9	320s (m=4, j=2, r=4, t_{exp}=10s)
		H		800s (m=4, j=5, r=4, t_{exp}=10s)
		z_{EMMI}	2008 Jan 30	2400s (r=4, t_{exp}=600s)
ULAS J0859 + 1010	LIRIS/WHT	H	2007 Dec 16	504s (j=9, r=14, t_{exp}=4s)
	LIRIS/WHT	$CH_4 l$	2007 Dec 16	450s (j=9, r=5, t_{exp}=10s)
	EMMI/NTT	z_{EMMI}	2007 Nov 17	600s (r=1, t_{exp}=600s)
ULAS J0938 − 0011	EMMI/NTT	z_{EMMI}	2008 Jan 29	1800s (r=3, t_{exp}=600s)
ULAS J0939 + 0016	EMMI/NTT	z_{EMMI}	2008 Jan 31	900s (r=2, t_{exp}=450s)
ULAS J0958 − 0039	LIRIS/WHT	J	2007 Mar 1	400s (j=5,r=2, t_{exp}=40s)
		H		600s (j=5,r=6, t_{exp}=20s)
		K_s		800s (j=5,r=8, t_{exp}=20s)
		z_{EMMI}	2008 Jan 30	2400s (r=4, t_{exp}=600s)
ULAS J1150 + 0949	LIRIS/WHT	J	2007 Mar 2	200s (j=5, t_{exp}=40s)
		H		1200s (j=5,r=12, t_{exp}=20s)
		K_s		1800s (j=5,r=19, t_{exp}=20s)
		Y		1200s (j=5,r=6, t_{exp}=40s)
		z_{EMMI}	2008 Jan 30	2400s (r=4, t_{exp}=600s)
ULAS J1157 + 0922[c]				
ULAS J1303 + 0016	LIRIS/WHT	J	2007 Mar 3	200s (j=5, t_{exp}=40s)
		H		1200s (j=5,r=12, t_{exp}=20s)
		K_s		1800s (j=5,r=18, t_{exp}=20s)
ULAS J1315 + 0826	LIRIS/WHT	J	2007 Mar 2	200s (j=5, t_{exp}=40s)
		H		400s (j=5,r=4, t_{exp}=20s)
		K_s		1000s (j=5,r=10, t_{exp}=20s)
		Y		1000s (j=5,r=5, t_{exp}=40s)
		z_{EMMI}	2008 Jan 31	2400s (r=4, t_{exp}=600s)
ULAS J1501 + 0822	LIRIS/WHT	J	2007 Mar 2	200s (j=5, t_{exp}=40s)
		H		400s (j=5,r=4, t_{exp}=20s)
		K_s		800s (j=5,r=8, t_{exp}=20s)
ULAS J1505 + 0703	UFTI/UKIRT	J	2007 Jul 23	540s (j=9, t_{exp}=60s)
		H		3240s (j=9, r=6, t_{exp}=60s)
		K		3240s (j=9, r=6, t_{exp}=60s)
		Y		2160s (j=5, r=2, t_{exp}=216s)
ULAS J1544 + 0819	UFTI/UKIRT	J	2007 Jul 15	300s (j=5, t_{exp}=60s)
		H		1800s (j=5, r=6, t_{exp}=60s)
		K		1800s (j=5, r=6, t_{exp}=60s)
		Y		1080s (j=5, t_{exp}=216s)
ULAS J1547 + 0053	LIRIS/WHT	J	2007 Mar 2	200s (j=5, t_{exp}=40s)
		H		600s (j=5,r=6, t_{exp}=20s)
		K_s		800s (j=5,r=8, t_{exp}=20s)
		Y		800s (j=5,r=4, t_{exp}=40s)
ULAS J0024 + 0022[b]	EMMI/NTT	z_{EMMI}	2007 Nov 16	2400s (r=4, t_{exp}=600s)
ULAS J0203 − 0102[b]	EMMI/NTT	z_{EMMI}	2007 Nov 17	1800s (r=3, t_{exp}=600s)

[a]Photometric observations consist of a combination of microsteps, jitters (or dithers), and repeats, of a single integration time (t_{exp}) that combine to give the total integration time (t_{int}). A microstep is an offset of a particular number (e.g. N+1/2) of pixels with respect to the current position.
[b]T dwarfs from Lodieu et al. (2007).
[c]No photometric follow-up was made of this T dwarf.

infrared and optical photometry for all 15 newly discovered T dwarfs is shown in Table 3, and their spectroscopic confirmation is discussed in Section 4. One of the remaining candidates has follow-up photometric colours that suggest it is an additional T dwarf (but no spectrum has been ob-

tained to date), and 18 candidates still await follow-up. Further discussion of the magnitude limited completeness of our follow-up will be presented in Section 6.

Table 3. T dwarf photometry and colours. Unless otherwise indicated, near infrared photometry was measured on the MKO system. Uncertainties are indicated in brackets as integer multiples of the last decimal place. The last two T dwarfs are from Lodieu et al. (2007), and here we present additional z-band measurements.

Name	Y	J	H	K	z	$Y-J$	$J-H$	$H-K$	$z-J$
ULAS J0222 − 0024	19.87±0.03	18.71±0.02	19.02±0.02	19.18±0.03	22.50±0.07[a]	1.16±0.04	-0.31±0.03	-0.16±0.04	3.79±0.07
ULAS J0823 + 0024	19.93±0.15[b]	18.57±0.05[b]	18.96±0.18[b]	18.58±0.23[b]	22.80±0.15	1.36±0.16	-0.39±0.19	0.38±0.29	4.23±0.16
ULAS J0837 − 0041	19.64±0.03[b]	18.52±0.09	18.60±0.11		22.18±0.06	1.12±0.09	-0.08±0.14		3.66±0.11
ULAS J0859 + 1010[c]	19.00±0.07[b]	17.88±0.06[b]	18.58±0.06	18.26±0.15[b]	21.53±0.05	1.12±0.09	-0.70±0.08	0.32±0.16	3.65±0.08
ULAS J0938 − 0011	19.83±0.12[b]	18.53±0.06[b]	19.00±0.19[b]		22.27±0.05	1.30±0.13	-0.47±0.20		3.74±0.08
ULAS J0939 + 0016	19.20±0.07[b]	17.96±0.03[b]	18.41±0.11[b]		21.74±0.05	1.24±0.08	-0.45±0.11		3.78±0.06
ULAS J0958 − 0039	19.88±0.15[b]	18.95±0.06	19.40±0.10	19.68±0.12[d]	22.85±0.09	0.93±0.16	-0.45±0.12	-0.28±0.16	3.90±0.10
ULAS J1150 + 0949	19.92±0.08[e]	18.68±0.04	19.23±0.06	19.06±0.05[d]	22.44±0.10	1.24±0.09	-0.55±0.07	0.17±0.08	3.76±0.11
ULAS J1157 + 0922	17.94±0.03[b]	16.81±0.01[b]	16.43±0.02[b]	16.24±0.04[b]		1.13±0.03	0.38±0.02	0.19±0.04	
ULAS J1303 + 0016	20.21±0.17[b]	19.02±0.03	19.49±0.09	20.10±0.17[d]		1.19±0.17	-0.47±0.09	-0.61±0.19	
ULAS J1315 + 0826	20.00±0.08[e]	18.86±0.04	19.50±0.10	19.60±0.12[d]	22.82±0.10	1.14±0.09	-0.64±0.11	-0.10±0.16	3.96±0.11
ULAS J1501 + 0822	19.70±0.15[b]	18.32±0.02	18.30±0.06	18.53±0.10[d]		1.38±0.15	0.02±0.06	-0.23±0.12	
ULAS J1505 + 0703	20.32±0.02	18.96±0.03	19.10±0.03	19.29±0.03		1.36±0.04	-0.14±0.04	-0.19±0.04	
ULAS J1544 + 0819	19.80±0.05	18.53±0.03	18.49±0.03	18.73±0.03		1.27±0.06	0.04±0.03	-0.24±0.04	
ULAS J1547 + 0053	19.37±0.06[e]	18.32±0.03	18.45±0.07	18.21±0.10[d]		1.05±0.07	-0.13±0.08	0.24±0.12	
ULAS J0024 + 0022[f]					22.77±0.10[a]				4.61±0.10
ULAS J0203 − 0102[f]					22.11±0.06[a]				4.07±0.06

[a] z_{EMMI} converted into z_{SDSS}.
[b] Photometry from the UKIDSS LAS.
[c] Also has a measured $H - CH_4l$ colour of -1.05±0.12, typical of mid-late T dwarfs.
[d] K_s(Liris) converted into K(MKO).
[e] z_{Liris} converted into Y(MKO).
[f] T dwarfs from Lodieu et al. (2007).

4 SPECTROSCOPIC OBSERVATIONS

Spectroscopic follow-up observations were made at five different facilities, providing a variety of near-infrared spectral ranges and sensitivities. Table 4 summarises which facilities were used to observe the newly confirmed T dwarfs in this work (as well as three candidates that were ruled out by spectroscopy), and gives details on the wavelength range covered, the date of the observations and the total exposure times used. A description of these facilities and the reduction methods we used is given in the next sections.

4.1 Gemini/GNIRS spectroscopy

The Gemini Near-Infrared Spectrograph (GNIRS; Elias et al. 2006) on Gemini South was used to make quick response observations, through programme GS-2007A-Q-15. GNIRS was used in cross-dispersed mode with the 32l mm^{-1} grism, the 1.0-arcsec slit and the short camera, to obtain 0.9–2.5μm R$\simeq$500 (per resolution element) spectra. The targets were nodded three arcsec along the slit in an ABBA pattern using individual exposure times of 240s. Calibrations were achieved using lamps in the on-telescope calibration unit. A0 and early F stars were observed as spectroscopic standards, either directly before or after the target observations, at an airmass that closely matched the mid-point airmass of the target, in order to remove the effects of telluric absorption. The observing conditions included some patchy cloud, seeing from 0.5–1.0 arcsec, and humidity ranging from 10–50 per cent.

Data reduction was initially implemented using tasks in the Gemini GNIRS IRAF (Image Reduction and Analysis Facility) package. Files were prepared and corrected for offset bias using NSPREPARE and NVNOISE, and order separation achieved with NSCUT. Each order was then median stacked at the A and B positions, and a difference image obtained using GEMARITH. Flat-field correction was not necessary since variations across the 6-arcsec slit are less than 0.1 per cent, and any flat-field variations in the dispersion direction will subsequently be removed when dividing by the spectrum of a standard. S-distortion correction and wavelength calibration were performed interactively using the telluric star spectra and argon arc lamp spectra, with NSAPPWAVE, NSSDIST and NSWAVE. Further reduction was carried out using custom written IDL (Interactive Data Language) routines. Apertures (1.5-arcsec wide) were centred on the spectra at the A and B positions, and the sky residuals were fit (and subtracted) using a surface constructed via a series of least-squares linear fits across the slit (excluding pixels within the apertures), with one fit for each spatial pixel row. Spectra were then extracted by summing within the A and B position apertures and combining. The target spectra were flux calibrated on a relative scale using the telluric standard spectra (after appropriate interpolation across any hydrogen absorption lines) with an assumed black-body function for T_{eff}=10000 and 7000 K for A0 and early F tellurics (e.g. Masana et al. 2006), respectively. The spectral orders were then trimmed of their noisiest portions, and the spectra normalized to unity at 1.27$\pm$0.005μm.

4.2 Gemini/NIRI spectroscopy

Gemini's Near Infrared Camera and Spectrometer (NIRI; Hodapp et al. 2003) was used, on the Gemini North Telescope on Mauna Kea, Hawaii, through programme GN-2007B-Q-26. NIRI was used in the f/6 mode with a 0.75 arcsec slit, and with the J grism (312.6 l mm^{-1}) and G0209 order sorting filter. This produced R$\sim$460 spectra over 1.05–1.41μm. The targets were nodded 10 arcsec along the slit in an ABBA pattern, and calibrations were achieved using argon lamp observations (as with GNIRS), and F stars as telluric standards. The observing conditions were very similar to those of the GNIRS observations.

NIRI data was reduced using tasks in the Gemini NIRI IRAF package. NRESID was used to create bad pixel masks from the individual flat-field observations. Combined flatfields were created with NSFLAT, and then bad-pixel removal and flat fielding of the science data was achieved using NSREDUCE. Sky removal was then carried out by subtracting consecutive AB pairs with GEMARITH, and multiple spectra combined with NSSTACK. We also minimised any pattern noise in our data using a custom written Python script, and wavelength calibrated with NSWAVE and corrected for any S-distortion with NSSDIST and NSTRANSFORM. Spectra were then extracted and calibrated using the same methods and software as were used for our GNIRS observations.

4.3 Subaru/IRCS spectroscopy

We used the Infrared Camera Spectrograph (IRCS; Kobayashi et al. 2000) on the Subaru Telescope on Mauna Kea, Hawaii. IRCS was used with its camera in the 52mas/pixel mode, and with the JH grism and a 0.6-arcsec slit. This resulted in R$\sim$100 spectra over a wavelength range of 1.0–1.6μm. The targets were nodded seven arcsec along the slit in an ABBA pattern. Calibrations were achieved using an argon lamp, and F2-5 stars were observed as telluric standards. The observing conditions were clear with seeing of $\sim$0.7 arcsec.

The IRCS data was reduced following the same reduction procedures as were used for our NIRI data, but using generic spectral reduction IRAF packages. The only practical difference was that S-distortion correction and wavelength calibration were done at the same time, using the TRANSFORM package. Arc observations were obtained several times throughout the night, and we performed wavelength calibration with the arc closest in time to each target observation. We estimate wavelength residuals (by intercomparing arcs) of $\sim$20Å which should not affect significantly our subsequent analysis.

4.4 UKIRT/UIST spectroscopy

One of the T dwarfs (ULAS J1157+0922) was observed at UKIRT using the UKIRT Imager Spectrometer (UIST; Ramsay Howat et al. 2004). The HK grism was used with the 4-pixel slit, giving a resolution R = 550. Individual exposure times on target were 240 s, and the target was nodded up and down the slit by 12 arcsec. The instrument calibration lamps were used to provide accurate flat-fielding and

Table 4. Spectroscopic observations. The table contains the new confirmed T dwarfs, as well as (at the bottom) three that we rule out with spectroscopy.

Name	Instrument & telescope	Wavelength range	UT date	t_{int}
ULAS J0222 − 0024	NIRI/Gemini-N	1.05-1.41μm	2 Sep 2007	960s (4×240s)
ULAS J0823 + 0024	NIRI/Gemini-N	1.05-1.41μm	2 Sep 2007	960s (4×240s)
ULAS J0837 − 0041	NIRI/Gemini-N	1.05-1.41μm	5 Oct 2007	960s (4×240s)
ULAS J0859 + 1010	NIRI/Gemini-N	1.05-1.41μm	2 Sep 2007	960s (4×240s)
ULAS J0938 − 0011	NIRI/Gemini-N	1.05-1.41μm	2 Sep 2007	960s (4×240s)
ULAS J0939 + 0016	NIRI/Gemini-N	1.05-1.41μm	2 Sep 2007	960s (4×240s)
ULAS J0958 − 0039	GNIRS/Gemini-S	0.9-2.5μm	4 Apr 2007	960s (4×240s)
ULAS J1150 + 0949	GNIRS/Gemini-S	0.9-2.5μm	10 Mar 2007	960s (4×240s)
ULAS J1157 + 0922	NICS/TNG	0.9-2.5μm	9 Apr 2007	1200s (4×300s)
	UIST/UKIRT	1.4-2.5μm	27 Jun 2007	5760s (24×240s)
ULAS J1303 + 0016	GNIRS/Gemini-S	0.9-2.5μm	10 Mar 2007	960s (4×240s)
ULAS J1315 + 0826	GNIRS/Gemini-S	0.9-2.5μm	4 Apr 2007	960s (4×240s)
ULAS J1501 + 0822	IRCS/Subaru	1-1.6μm	1 Jul 2007	2400s (8×300s)
ULAS J1505 + 0703	NIRI/Gemini-N	1.05-1.41μm	22 Aug 2007	1200s (4×300s)
ULAS J1544 + 0819	NIRI/Gemini-N	1.05-1.41μm	4 Sep 2007	960s (4×240s)
ULAS J1547 + 0053	IRCS/Subaru	1-1.6μm	1 Jul 2007	1920s (8×240s)
ULAS J0039 + 0002	IRCS/Subaru	1-1.6μm	1 Jul 2007	1920s (8×240s)
ULAS J1301 + 0023	IRCS/Subaru	1-1.6μm	1 Jul 2007	1920s (8×240s)
ULAS J2243 − 0046	IRCS/Subaru	1-1.6μm	1 Jul 2007	1920s (8×240s)

wavelength calibration. The F5V star HD 96218 was observed prior to the target to remove the effects of telluric absorption, and to provide an approximate flux calibration. Relative flux calibration was improved by scaling the spectra to the H and K magnitudes measured in the LAS, and finally we scaled the spectra at 1.6μm to join onto our broader wavelength TNG spectra (see next section).

4.5   TNG/NICS spectroscopy

We have also obtained a low-resolution (R∼50) near-infrared (0.9–2.5μm) spectrum of ULAS J1157+0922 with the Near Infrared Camera Spectrometer (NICS; Baffa et al. 2001) on the Telescope Nazionale Galileo (TNG). The observations were made in service mode by the TNG staff, with seeing in the 1.2–2.0 arcsec range. NICS is a multi-purpose instrument equipped with a HgCdTe Hawaii 1024x1024 detector with 0.25 arcsec per pixel, yielding a 4.2 by 4.2 arcmin field-of-view. We employed the Amici mode with a one arcsec slit, yielding a wavelength coverage of 0.9–2.5 μm. Four integrations of 300 sec were taken for the target in an ABBA dither pattern. A and B spectra were averaged, differenced, and the resulting image flat-fielded. A one-dimensional spectrum was then extracted with the IRAF task APSUM. A standard star (HIP48971; A0) was observed immediately after the target at a similar airmass, and divided through the science target to correct for telluric absorption, before flux calibrating with a black-body of the same T_{eff} as the A0 star. Due to the low resolution of the Amici mode, virtually all the Ar/Xe arc lines are blended and cannot be easily used for standard reduction procedures. For this reason, wavelength calibration was performed in a NICS-specific way, using a look-up table (of wavelength against pixel) based on the instrument's theoretical dispersion from ray-tracing. This first-pass wavelength calibration was then offset to best fit the observed

spectra of the calibration sources. No attempt was made to correct the very modest level of slit curvature.

4.6   Spectral classification

Figure 3 shows the spectra of the 15 new T dwarfs. For each spectrum we calculated all available near-infrared spectral indices from B06; H2O-J, CH4-J, H2O-H, CH4-H and CH4-K. For the GNIRS and NICS spectra we were able to measure all five ratios. For the IRCS spectra we were able to measure H$_2$O-J, CH$_4$-J and H$_2$O-H. The NIRI spectra allowed us to measure the H$_2$O-J and CH$_4$-J, and the UIST spectrum covered H$_2$O-H, CH$_4$-H and CH$_4$-K. We also compared the data by eye to template spectra of T dwarfs defined by B06 as standard T4, T5, T6, T7 and T8 types. The results for the new T dwarfs are given in Table 5. Some scatter is present in the spectral indices given in Table 5 due to low signal-to-noise ratio. Consequently, the direct comparison with templates has been given more weight than the spectral indices in the assignment of spectral types, and the adopted uncertainty in Table 5 reflects the range in type implied by this comparison. Note also that in the case of one object (ULAS J1150 + 0949), the H$_2$O-H spectral ratio indicates a significantly earlier spectral type (T3) than all the other ratios for this object (T6-7), and we have thus typed it as T6.5p. Table 5 also presents distance estimates for the T dwarfs based on their spectral type and J-band brightness, using the M_J spectral type relation (excluding known and possible binaries) of Liu et al. (2006), and allowing for the rms scatter in this relation.

Figure 4 shows the Subaru spectra of the three candidate T dwarfs that we rule out with spectroscopy. Clearly none of these objects show the strong H$_2$O and CH$_4$ absorption at 1.1–1.2μm and 1.3–1.5μm that sculpts the $J-$band and $H-$band peaks characteristic of T dwarfs. After allowing for some residual telluric noise at ∼1.4μm, the spectrum
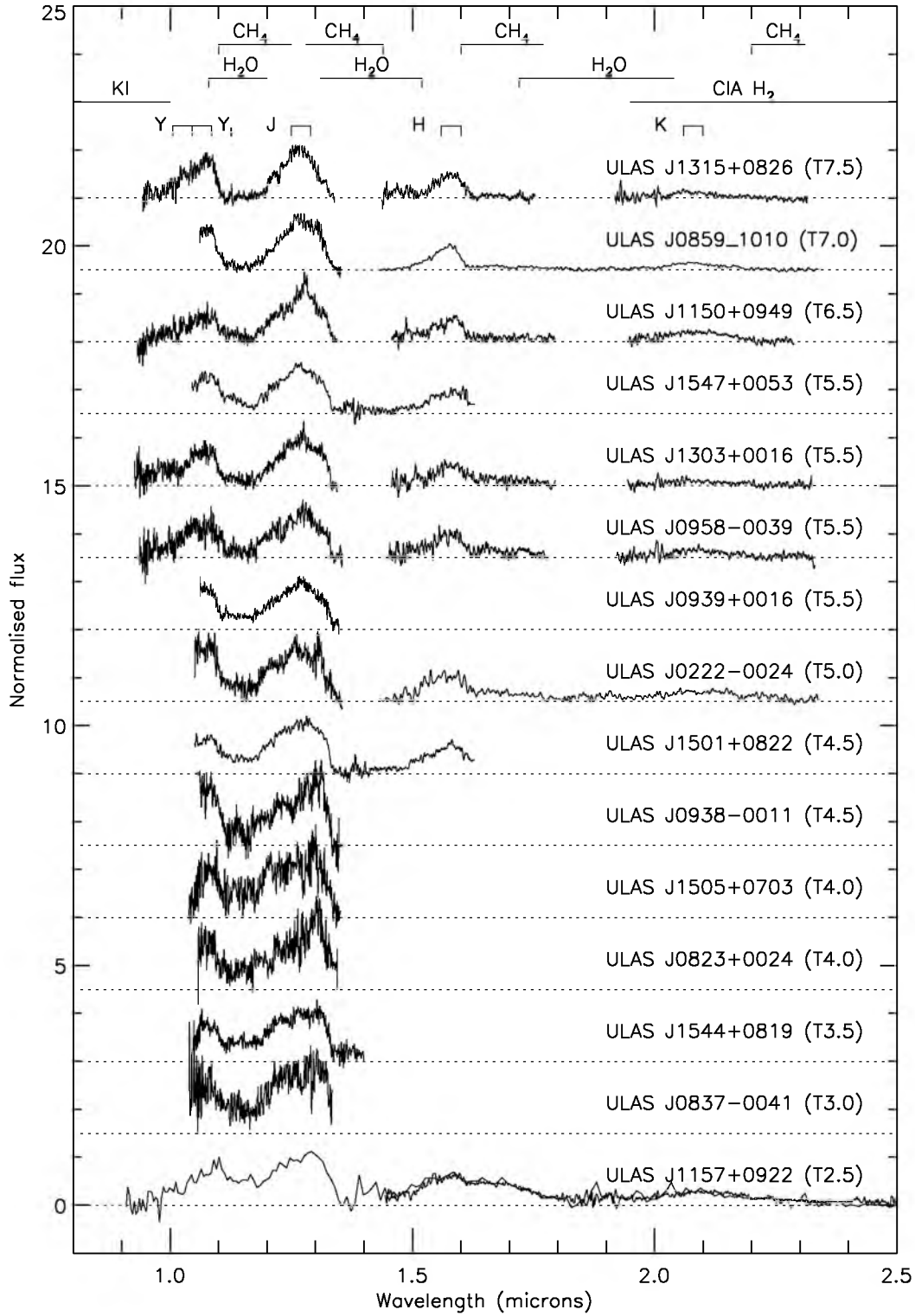
Figure 3. Spectra of the 15 new T dwarfs. The spectra are all normalised to unity at $1.27\pm0.005\mu$m. Defining features of T dwarf spectra are indicated. Also shown are the Y, Y_l, J, H and K bands which we use to calculate spectral peak ratios (see Section 5).

Table 5. Spectral types derived from indices and by comparison with T dwarf templates (following B06).

Name	H_2O-J	CH_4-J	H_2O-H	CH_4-H	CH_4-K	Template	Adopted	Distance[a] (pc)
ULAS J0222 − 0024	0.272 (T5)	0.368 (T5.5)				T5	T5.0±0.5	55-78
ULAS J0823 + 0024	0.390 (T3)	0.696 (T1)				T4±1	T4±1	55-78
ULAS J0837 − 0041	0.419 (T3)	0.660 (T2)				T3	T3.0±0.5	54-76
ULAS J0859 + 1010	0.058 (T8)	0.266 (T7)				T7	T7±0.5	26-36
ULAS J0938 − 0011	0.190 (T6)	0.484 (T4)				T4.5	T4.5±0.5	53-75
ULAS J0939 + 0016	0.288 (T5)	0.366 (T5)				T5-6	T5.5±0.5	37-52
ULAS J0958 − 0039	0.125 (T6.5)	0.341 (T5.5)	0.391 (T4)	0.402 (T5)	0.130 (T6.5)	T5.5±1	T5.5±0.5	58-82
ULAS J1150 + 0949	0.087 (T7)	0.302 (T6.5)	0.455 (T3)	0.230 (T6.5)	0.032 (≥T7)	T6-7	T6.5p±0.5	42-60
ULAS J1157 + 0922	0.428 (T3)	0.544 (T3)	0.453 (T3)	0.772 (T3)	0.557 (T2)	T2	T2.5±0.5	24-34
ULAS J1303 + 0016	0.105 (T7)	0.324 (T6)	0.332 (T5.5)	0.367 (T5.5)	0.025 (≥T7)	T5-6	T5.5±0.5	60-85
ULAS J1315 + 0826	0.034 (T8)	0.181 (T8)	0.227 (T7)	0.121 (T8)	0.080 (>T7)	T8	T7.5±0.5	34-48
ULAS J1501 + 0822	0.290 (T5)	0.418 (T5)	0.411 (T4)			T4-5	T4.5±0.5	48-68
ULAS J1505 + 0703	0.349 (T4)	0.572 (T2.5)				T4±1	T4.0±0.5	66-93
ULAS J1544 + 0819	0.411 (T3)	0.520 (T3.5)				T3.5	T3.5±0.5	55-77
ULAS J1547 + 0053	0.217 (T5)	0.363 (T5)	0.331 (T5)			T5-6	T5.5±0.5	44-61

[a] Assumes single objects.
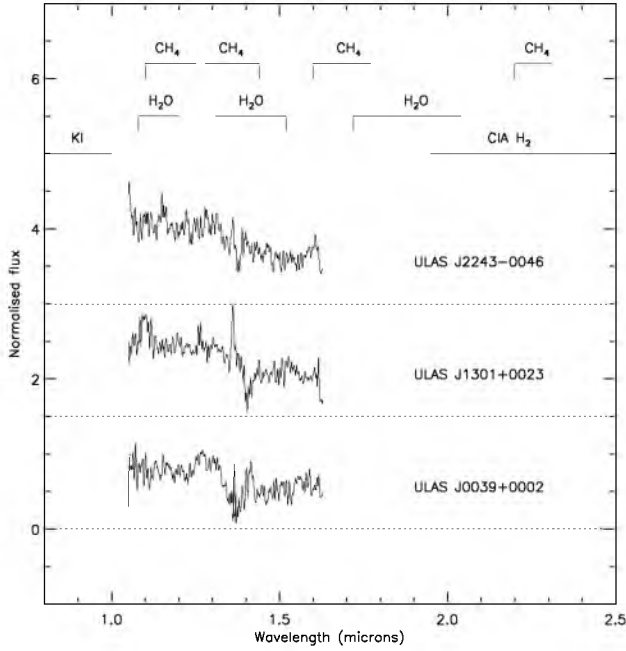
Figure 4. Spectra of the three T dwarf candidates ruled out with spectroscopy. The absorption feature that we expect to define T dwarf spectra are indicated, and are clearly not present in these spectra.

of ULAS J2243-0046 appears to have the form of a blue continuum. The other two sources show evidence of H_2O absorption at 1.3–1.4μm, and appear to be M dwarfs. The LAS YJ and HK photometry used to select these candidates was taken on two separated nights, and variability might explain how some M dwarfs can appear to have blue $J − H$ colours. ULAS J1301+0023 also showed some evidence for possible methane absorption (at the ∼1–2σ level) via narrow-band CH_4s- and CH_4l-band photometry (Kendall et al. 2007). Our spectrum of this object does not cover the full wavelength range of these filters (1.53–1.63μm and 1.64–1.74μm respectively), so we cannot rule out an intrinsically blue methane

(CH_4s-CH_4l) colour. However, it may simply be that the relatively low signal-to-noise ratio of the narrow-band photometry led directly to the measurement of a blue colour.

5 T DWARF PROPERTIES

We now consider the overall spectral morphology of the T dwarfs using both their spectra and their photometric properties. We measured the relative brightness of the $Y−$, $J−$, $H−$, and $K−$band spectral peaks by summing flux in several bands. In general we used the bands defined by Burgasser, Burrows & Kirkpatrick (2006), to which we also add an additional $Y−$band at a slightly longer wavelength (which we refer to as Y_l). Our $Y−$, Y_l-, $J−$, $H−$, and $K−$band spectral peaks cover the 1.005–1.045, 1.045–1.085, 1.25–1.29, 1.56–1.60, and 2.06–2.10μm wavelength ranges respectively, and are indicated in Figure 5. Table 6 shows the integrated flux peak ratios for the 15 new T dwarfs. We were able to measure the Y_l/J ratio for all our T dwarf spectra, while the short wavelength cut-off in the spectral coverage of several of the T dwarfs precludes the measurement of the Y/J ratio.

To assess how the spectral morphology of the T dwarfs may depend on their physical properties, we compare our observed properties with the predictions of model atmospheres. As a primary comparison we use the BT-Settl models (which combine with structure models to give the Lyon-Settl models shown in Figure 1), generated with version 15.3 of the general-purpose stellar atmosphere code Phoenix (Hauschildt & Baron 1999). These models use a set-up that currently gives the best BT-Settl fits to observed spectra of M, L and T dwarfs, updating the micro-physics used in the GAIA model grid (Kucinskas et al. 2005, 2006). For a summary of the important input physics of these models, see Warren et al. (2007a). Note that Burgasser, Burrows & Kirkpatrick (2006) and Leggett et al. (2007) have also examined these effects in the spectral models of Burrows et al. (2006; Tucson models) and Marley et al. (in prep.; AMES models), and while the different model trends in spectral morphology are in broad agreement, we highlight any differences between these model sets and the BT-Settl models.

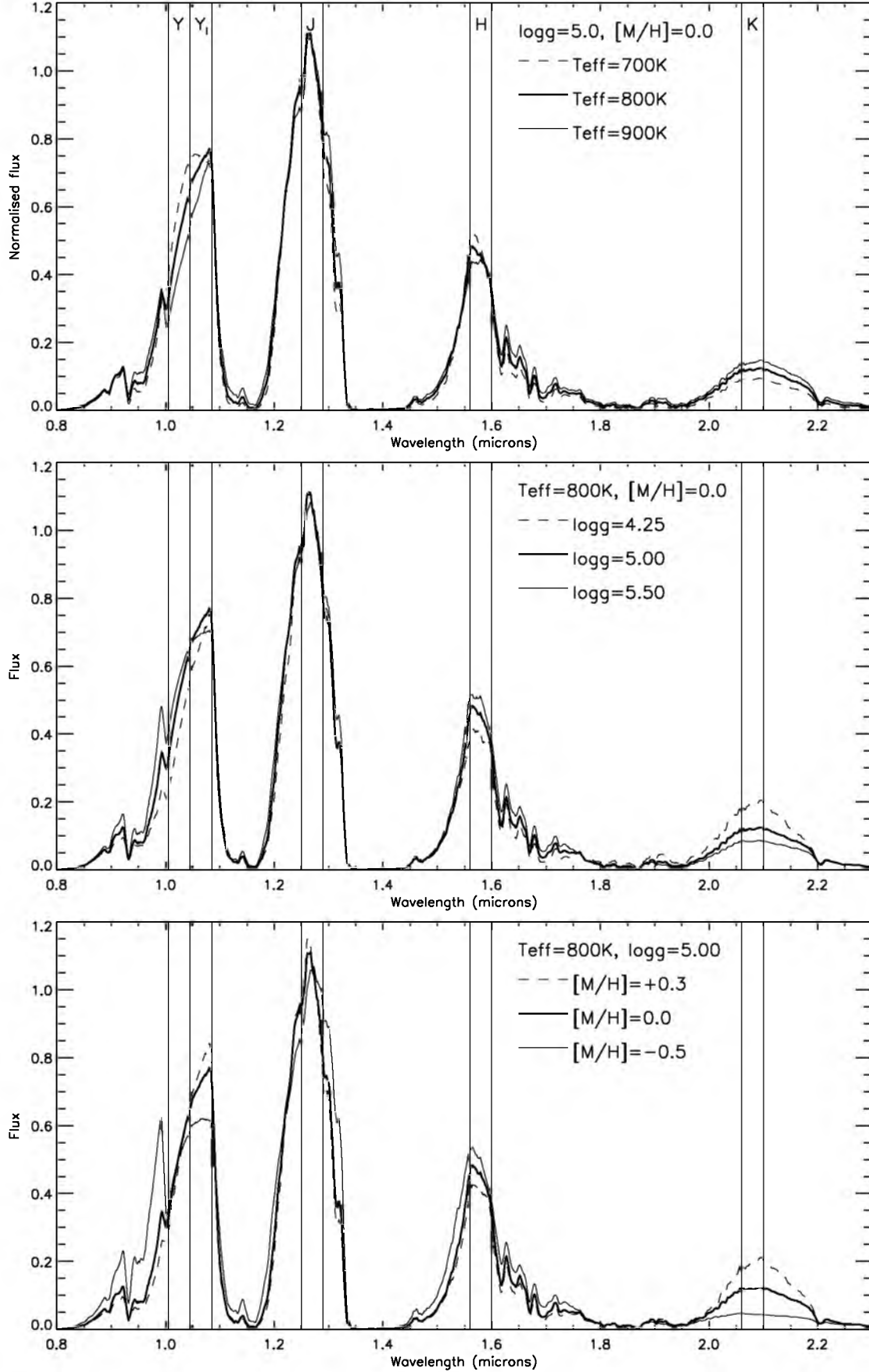Figure 5 demonstrates how the BT-Settl model spectra

Figure 5. Model BT-Settle T dwarf spectra showing theoretical T_{eff}, $\log g$ and [M/H] variations.

Table 6. Ratios of spectral peaks.

Name	SpT	Y/J	Y_l/J	H/J	K/J	K/H	Unusual property?
ULAS J0222 − 0024	T5.0	-	0.997	-	-	-	Noisy - possibly unusual metallicity
ULAS J0823 + 0024	T4.0	-	0.892	-	-	-	Normal
ULAS J0837 − 0041	T3.0	-	0.833	-	-	-	Normal
ULAS J0859 + 1010	T7.0	-	0.814	-	-	-	Normal
ULAS J0938 − 0011	T4.5	-	1.195	-	-	-	Noisy - possibly unusual metallicity
ULAS J0939 + 0016	T5.5	-	0.918	-	-	-	Normal
ULAS J0958 − 0039	T5.5	0.488	0.708	0.521	0.182	0.349	Noisy - possibly low $T_{\rm eff}$ or unusual metallicity
ULAS J1150 + 0949	T6.5	0.299	0.467	0.428	0.199	0.465	Low-gravity[a]
ULAS J1157 + 0922	T2.5	0.401	0.467	0.652	0.291	0.446	Normal
ULAS J1303 + 0016	T5.5	0.416	0.738	0.449	0.110	0.245	High gravity
ULAS J1315 + 0826	T7.5	0.436	0.723	0.472	0.122	0.258	Normal
ULAS J1501 + 0822	T4.5	-	0.658	0.526	-	-	Normal
ULAS J1505 + 0703	T4.0	-	0.710	-	-	-	Normal
ULAS J1544 + 0819	T3.5	-	0.638	-	-	-	Normal
ULAS J1547 + 0053	T5.5	-	0.739	0.437	-	-	High gravity[b]

[a]Possibly high [M/H] as well.
[b]From photometric colour only.

change with $T_{\rm eff}$, gravity, and metallicity. Our baseline properties in this figure are $T_{\rm eff}$=800K, log g=5.0, [M/H]=0.0, and spectral variations for ±100K, $^{+0.5}_{-0.75}$ dex, and $^{+0.3}_{-0.5}$ dex in $T_{\rm eff}$, log g and [M/H] respectively, are shown. The spectra have been normalised to unity in the peak of the J-band. As has been noted previously for the Tucson and AMES models, $T_{\rm eff}$ variations are significant in the wings of the H-band peak and in the peak of the K-band. The BT-Settl models also suggest that the Y-band peak has some $T_{\rm eff}$ sensitivity, with increasing and decreasing $T_{\rm eff}$ suppressing and enhancing the Y-band flux (with respect to the $J-$band peak) respectively. By comparison the Tucson models also exhibit some Y-band variation with $T_{\rm eff}$, but in the opposite sense to that of the BT-Settl models, and the AMES models show little variation with $T_{\rm eff}$ (Leggett et al. 2007). Gravity has a significant effect on the model K-band peak, with higher log g causing K-band suppression and lower log g enhancing the K-band flux. Some observational evidence may also support this trend, as for example, S Ori 70 (a possible T5.5 member of the ~3Myr σOrionis cluster; Zapatero-Osorio et al. 2008), and PLZJ93 (a possible T3-5 member of the Pleiades open cluster; Casewell et al. 2007) both show a strong $K-$band enhancement, which would presumably result from the low surface gravity of members of these solar metallicity clusters.

In addition, the BT-Settl Y-band flux is suppressed to some extent at lower gravity. However, this effect is not predicted by the Tucson or AMES models (with both models showing an increase in flux for lower gravity), and this trend is thus ambiguous when taking all models into consideration. Metallicity affects the K-band peak in a similar way to gravity, where increasing and decreasing metallicity causes K-band enhancement and suppression respectively. Indeed, K-band fluxes may be quite sensitive to even small metallicity differences, as suggested by Liu, Leggett & Chiu (2007) when comparing the spectra of HD 3651B (Burgasser 2007) and Gl570D. Also, metallicity affects the Y-band flux peak significantly. This effect is also seen for the other models, although it is not clear how the Y-band peak should

change. The Tucson and AMES models suggest that Y-band suppression could occur at higher metallicity, although the BT-Settl models suggest that some enhancement may occur (at the expense of shorter wavelength flux).

We do not make direct comparison to the model predictions, but instead identify T dwarfs whose relative flux peak ratios and/or colours are unusual in the context of T dwarf properties typical of the solar neighborhood. We compared the measurements of the T dwarfs with previous samples (from Knapp et al. 2004; Golimowski et al. 2004; Chiu et al. 2006), and found that most of the sample (eleven out of fifteen) have ratios that appear consistent with the majority of solar neighborhood T dwarfs. However, there are some notable exceptions.

• ULAS J0222-0024 and ULAS J0938-0011 appear to show Y_l enhancement. While our spectral coverage only allowed us to measure the Y_l/J flux ratio of ULAS J0222-0024 and ULAS J0938-0011, the strongly enhanced flux in the Y-peak is suggestive of unusual metallicity. However, there is no evidence for an enhanced Y flux from the $Y - J$ colours. It is possible that the Y_l-band (but not the $Y-$band) could be enhanced for these objects. This would be consistent with the BT-Settl model predictions for a high metallicity object (see Figure 5), but the Y spectra of these objects are somewhat noisy and more spectral coverage would be needed to properly confirm this.

• ULAS J0958-0039 may show some Y-band and H-band enhancement, although the somewhat noisy nature of this object's spectrum make this result rather tentative. However, it is supported by the relatively blue $Y - J$ colour of this object. Although note that the Y_l/J spectral ratio of this object is not unusual. Consideration of the models suggests that such an effect could arise from lower $T_{\rm eff}$ or unusual [M/H], but it is not currently clear if either or both of these effects are responsible.

• ULAS J1150+0949 shows strong Y and Y_l suppression and also an enhanced K-band flux. The enhanced K/H ratio and relatively red $H - K$ colour is suggestive of low gravity. The suppressed Y-band flux for this object also points to

low gravity when one considers the BT-Settl models. However, note that the Tucson and AMES models (which show no significant Y-band gravity sensitivity) could invoke an increase in metallicity to explain this Y-band suppression. While it seems simpler to require only one non-typical property to explain the unusual flux peak ratios, it is not possible to make firm conclusions at this stage, in light of the model ambiguities. ULAS J0859+1010 also has suppressed Y_l flux and unusually red $H - K$ colour, and could have similar physical properties to ULAS J1150+0949.

• ULAS J1303+0016 shows strong K-band suppression and very blue $H-K$ and $J-K$ colours, but has a normal Y-band flux peak. This is consistent with the predicted model trends for a high gravity object.

• Finally, ULAS J1547+0053 shows typical Y_l/J and H/J spectral ratios, but has unusually red $J - K$ and $H - K$ colours. Like ULAS J1150+0949 this object may have low gravity, although it does not show suppressed Y_l flux.

We summarise the above discussion in the last column of Table 6, where we indicate possible non-typical properties that might explain the observed spectral morphology and colours.

5.1 Searching for the lowest $T_{\rm eff}$ objects

Figure 6 shows the available colours of our new T dwarfs as well as other T dwarfs that have been discovered or recovered in the LAS (Geballe et al. 2002; Kendall et al. 2007; Lodieu et al. 2007; Warren et al. 2007a; Chiu et al. 2007), including an additional T8+ object CFBDS0059, recently discovered using the Canada-France-Hawaii Telescope (Delorme et al. 2008) and independently identified in the LAS. Different T dwarf spectral types are indicated with different symbols (see the key in the top right plot). Also shown are the sample of DR2 L dwarf candidates (plus signs; see Section 2.1), and the sample of typical brighter sources from the LAS (points; see section 2.1) for comparison. Our YJH selection box is indicated with a dotted line.

Examination of the plots shows several interesting features. For the blue T dwarfs (contained in our selection box) there is some evidence for a possible trend in $Y - J$ colour as one moves from the T0-4.5 dwarfs to the T5-8 dwarfs. This trend may be continuing into the T8+ objects, as suggested by the rather bluer colour of the T8.5 dwarfs ULAS J0034-0052 and CFBDS0059 (filled circles). The $J - H$ colours of T dwarfs generally get bluer out to spectral types of T8, although the two T8+ dwarfs do not have very blue $J - H$. The $H - K$ and $J - K$ colours show strong variations irrespective of spectral sub-class, due presumably to variation in surface gravity and metallicity, and such variations appear to continue into the T8+ range. As such, these colours may not be strong indicators of T8+ types in themselves, although models do indicate that when combined with certain spectroscopic information (e.g. W_J index describing the width of the J-band peak) such colours (or flux ratios) can provide useful $T_{\rm eff}$ constraints (see fig 7 of Warren et al. 2007 and fig 6 of Delorme et al. 2008). The $z - J$ colour is clearly rather scattered for T dwarfs, and there is certainly no evidence in Figure 6 for T dwarfs becoming redder in $z - J$ at lower $T_{\rm eff}$. However, it is interesting to note that the $z - J$

colour of the two T8+ dwarfs is perhaps slightly bluer than other mid-late T dwarfs.

Although only two T8+ dwarfs are currently known, their colours suggests that $Y - J$ may be a particularly useful colour for identification. The $J - H$ colour shows no evidence so far for getting bluer beyond T8, however this is based on only two objects, and we cannot rule out the possibility that the small number of T8+ dwarfs discovered so far could be unusual. A young (still contracting) brown dwarf for instance, would be brighter than an older counterpart of the same $T_{\rm eff}$, and hence detectable to greater distance. This could provide an explanation as to why the first discoveries in this new $T_{\rm eff}$ range might have non-typical spectral properties. Clearly a larger sample of T8+ dwarfs is needed to properly understand their range of spectral properties. To this end, it could prove desirable to extend LAS searches for the lowest $T_{\rm eff}$ objects to even bluer $Y - J$ colours, and possibly redder $J - H$. Optical constraints (e.g. non-detections) would be particularly important as the near infrared colours of candidates become more akin to those of hot stars, but the capabilities of UKIDSS and SDSS combine to give great potential for such searches.

6 T DWARF NUMBERS

In this section we discuss the sample of LAS T dwarfs identified thus far in DR1 and DR2, and place a magnitude limited constraint on T dwarf numbers in this 280 sq degs of the LAS. We discuss various completeness issues, and make approximate corrections to the T dwarf statistics to account for these.

We first consider the completeness with which we have followed up candidates from DR1 and DR2. Overall we have followed up 82 per cent of all our $J \leqslant 19.5$ candidates (see Section 3). Nearly all those that still require follow-up are fainter than $J=19$. Of the 44 initial candidates with $J \leqslant 19.0$, 42 have reliable classifications. The follow-up presented here combined with the previous observations reported by Kendall et al. (2007), Lodieu et al. (2007), Warren et al (2007a), and Chiu et al. (2007), have resulted in the discovery of 23 T dwarfs with $J - H \leqslant 0.1$ in the LAS DR2 sky. Of these, 22 T dwarfs have $J \leqslant 19.0$ (10 with $J < 18.5$ and 12 with $J=18.5$-19.0). Since an extra half a magnitude depth should double the surveyed volume, it can be seen that our sample shows statistical evidence for a good level of completion down to $J=19.0$.

The spread in colour of known T dwarfs means that our colour selection ($J-H \leqslant 0.1$) will thoroughly probe only certain ranges of T spectral class, and for some sub-type ranges a fraction of the T dwarfs will be missed. To assess the spectral type range that our colour selection probes, we used the population of optically selected SDSS T dwarfs[1] (to avoid NIR colour selection effects). SDSS T dwarf searches reach $z=20.4$, and should thus be complete across the T range ($z - J \sim 3$–4) to $J \sim 16.4$. There are currently 19 SDSS T dwarfs with $J < 16.4$ and $J - H_{MKO} > 0.1$ which have been found in 6600 sq degs of sky (see Chiu et al. 2007 and references therein). Amongst these, 14 have spectral type T0–

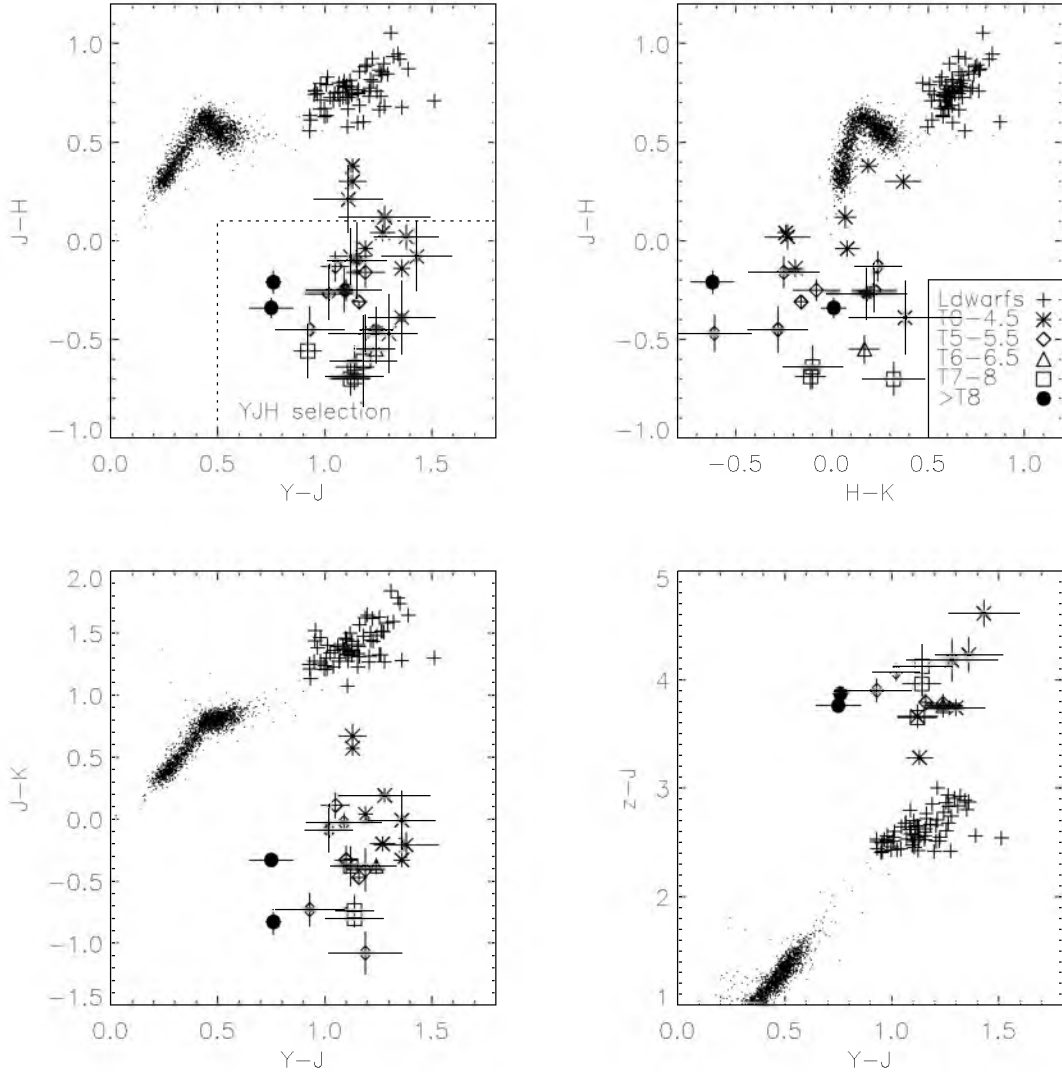[1] From the DwarfArchives.org site, http://dwarfarchives.org

Figure 6. A series of two-colour diagrams showing the known LAS T dwarfs, including those first presented by Geballe et al. (2002), Kendall et al. (2007), Lodieu et al. (2007), Warren et al. (2007a), Chiu et al. (2007), and this work.

2 and five have spectral type T2.5–3.5. None have a spectral type of T4 or greater. Correcting these numbers to a LAS $J=19$ depth and sky coverage reveals that although we would not expect to have missed a significant number of $\geqslant$T4 dwarfs, we would expect to have missed $\sim$21 T0-2 dwarfs and approximately eight T2.5–3.5 dwarfs. Clearly our search should be essentially complete for spectral types $\geqslant$T4, but a correction would be necessary if considering spectral type ranges that include earlier T dwarfs. Table 7 shows how this correction factor changes for different ranges of T spectral class, and how the over-all expected numbers of T dwarfs would be affected.

To take advantage of our good level of completeness and facilitate simple comparison with the theoretical predictions using the methods of Deacon & Hambly (2006), we specifically consider the spectral type range T4 and later. Allowing for the two outstanding candidates we place a constraint of 19–21 T4-T8.5 dwarfs with measured $J-H \leqslant 0.1$ and $J \leqslant 19$

in the LAS Dr2 sky, and allow for a additional 10% Poisson uncertainty on the upper limit to account for the limited statistical accuracy of our SDSS sample analysis.

To account for measurement uncertainties, we have estimated the number of $\geqslant$T4 dwarfs with intrinsic $J-H \leqslant 0.1$ whose colour may have been statistically scattered out of the selection region. To do this we estimated (for each $\geqslant$T4 dwarf discovered via YJH detection) the probability that $J-H$ colours could have been scattered sufficiently red-ward from the LAS measured value, taking into account the 1-σ uncertainties on their measured colour. Probabilities were then summed, and our result suggests that we would only expect $\sim$1.5 $\geqslant$T4 dwarfs to be missed in this way.

In addition, we account for some level of unresolved binarity amongst the LAS T dwarfs. Unresolved binaries will be brighter than a single T dwarf population, and could thus be found in a larger volume of sky. A correction is necessary if one wishes to compare T dwarf numbers with

theoretical predictions for the total number of individual T dwarfs. Brown dwarf binaries are generally tight systems (e.g. <15AU; Reid et al. 2006), of approximately near equal mass components. A volume limited sub-stellar binary fraction (BF) has been reported with values ranging from 10–50 per cent via open cluster photometry and high resolution imaging (e.g. Burgasser et al. 2003; Pinfield et al. 2003; Lodieu et al. 2007), where

$$BF = \frac{N_b}{N_b + N_s},\qquad(1)$$

N_b and N_s being the number of binary and single systems respectively. If one makes the simplifying assumption of binary components of equal brightness (see Burgasser et al. 2003 for a more generalised conversion for a range of mass-ratio distributions; e.g. Allen 2007), then the relative number of binary and single systems in a magnitude limited sample will be

$$\frac{N_b}{N_s} = \frac{2\sqrt{2}BF}{1 - BF},\qquad(2)$$

and the number of binary systems (compared to the total magnitude limited number of systems N_m) will be

$$N_b = \left(\frac{2\sqrt{2}}{2\sqrt{2} + \frac{1}{BF} - 1}\right)N_m.\qquad(3)$$

For BF=10–50%, we thus estimate that 24–74 per cent of the sources in our magnitude limited sample could be unresolved binaries. Of these unresolved binaries systems, only ∼35 per cent ($1/2\sqrt{2}$×100%) would be included in our $J \leqslant 19$ sample if the binary components were resolvable (i.e. if the combined binary J-band brightness is >18.25 then the individual T dwarf components would have $J >19$ and would be excluded from our sample). However, for the $J \leqslant 18.25$ unresolved binary systems, we must count both of the T dwarf components. We thus derive a binarity correction factor of 0.76–0.93 (for BF=10–50 per cent respectively) to correct our numbers to represent a magnitude limited sample of individual T dwarfs. Note that despite a wide range in BF, this binary correction factor has a relatively small range.

We also account for spatial incompleteness which can result from the way in which optical catalogues are used to inform candidate selection. In our initial selection, a nearby optical source might result in a candidate being rejected if it was close enough to mascarade as an optical counterpart, making the candidate appear too bluer in its optical-infrared colour. This effectively decreases the search area by some fraction that is dependent on the source density and the search criteria used. We account for this with a correction factor (ϵ) that is the ratio of clear sky (unaffected by optical mis-matches) to total sky considered (A_{tot}), and can be derived from probability analysis as,

$$\epsilon = \left(1 - \frac{\sigma}{A_{tot}}\right)^N,\qquad(4)$$

where σ is the area excluded by a single optical source and N is the number of optical sources in the area considered. For 1 deg^2 this reduces to $\epsilon = (1 - \sigma)^n$ where n is the number density of optical sources. Figure 7 shows ϵ plotted against source density for our search of the LAS (solid line) as well as for previous searches of 2MASS (dashed line, e.g.
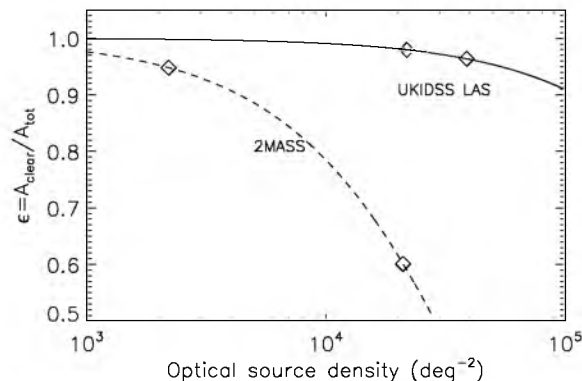

Figure 7. Predicted area corrections, $\epsilon = \frac{A_{clear}}{A_{tot}}$ for excluding regions around optical sources as a function of source density. The UKIDSS LAS exclusion regions comprise 2 arcsec radii circles centred on SDSS sources, and for comparison the 2MASS exclusion regions comprise 10 arcsec radii circles centred on USNO sources. The source densities inherent in our search and in previous 2MASS searches out of the plane are enclosed by open diamonds.

Burgasser et al. 2004). The differences result from the different exclusion regions used, which extended out to 10 arcsecs from any USNO-A2.0 optical source for 2MASS searches, but only extend out to 2 arcsecs from any SDSS source for our search of the LAS. The full effect of this incompleteness depends on the number density of optical sources in the regions of sky being considered, and this in turn is dependent on the galactic latitude. LAS DR2 extends across the $b =$20-80 deg range, although is mostly concentrated in $b =$40-75 deg. The SDSS source number density ranges from ∼20,000-40,000 sources per square degree over the LAS DR2 sky (indicated by open diamonds in Figure 7), and as can be seen, this results in a range of ϵ=0.96-0.98.

For the 2MASS comparison, despite the optical surveys being shallower than SDSS, the larger exclusion regions (with 10 arcsec radii) combined with the greater range of galactic latitude searched (reaching $|b| = 15$) result in the ϵ correction having a potentially much greater impact than it does for the LAS DR2 T dwarf sample. We chose to factor in a 3% increase to our T dwarf numbers to account for this spatial incompleteness effect, but note that this small correction has no significant effect on our results.

Finally, we account for Malmquist bias. We first consider the effect of an intrinsic scatter in the M_J of T dwarfs (classical Malmquist bias). This scatter will cause the J-band magnitude limited sample to probe different volumes for any fixed spectral type. Those T dwarfs that are intrinsically brighter than average (for their type) will be sampled from a larger volume than those that are fainter. This will bias the mean M_J to brighter values, and effectively result in the overall sample coming from a larger volume than if the T dwarfs had a non scattered M_J-spectral type relation. Assuming a uniform space density and ignoring any effects of slope in the substellar luminosity function (i.e. $d\phi/dM = 0$), the fractional increase in the measured number of T dwarfs (ϕ) is given by

$$\frac{\Delta\phi}{\phi} = \left(\frac{0.6\sigma}{\log e}\right)^2\qquad(5)$$

where σ is the rms dispersion (assuming a Gaussian distribution) of T dwarf absolute magnitudes. We estimated this scatter using the sample of T dwarfs with parallax measurements presented by Liu et al. (2006) combined with their polynomial fit (M_J-spectral type) to the single T dwarfs (ignoring known and possible unresolved binaries). When one considers only the subset of T dwarfs with spectral type $\geqslant$T4 (i.e. matched to the DR2 sample), the rms scatter from the best-fit polynomial is σ=0.29, resulting in an increased volume of $\Delta\phi/\phi$=16%. We thus decreased our T dwarf numbers to account for this bias.

An additional Malmquist effect results from photometric uncertainty near the sample limit, since more T dwarfs scatter into the sample from fainter magnitude (i.e. at a greater distance, in a larger volume) than scatter out of it. However, since we measured accurate follow-up photometry for the majority of our initial candidates (down to J=19.5) before we imposed the J=19.0 cut considered here, the effective scatter at the J=19 limit will be small. We conservatively estimate this scatter to be σ=0.05, and expect a resulting Malmquist correction of no more than 0.5% which is insignificant.

Our final magnitude limited T dwarf number constraints take account of the above corrections, and assumes Poisson uncertainties associated with sample sizes. We thus estimate that there are 17±4 single $\geqslant$T4 dwarfs with J <19 in the 280 sq degs of Dr2 sky. Table 7 also presents the number constraints derived using different lower limits for the spectral type range.

For comparison, we undertook a series of simulations based on those presented in Deacon & Hambly (2006). These were scaled to take into account the difference in size between the full LAS and DR2. The J-band depth limit was set to 19, and the Y-band depth limit to 20. This Y-band depth limit is actually 0.2 magnitudes brighter than the 5σ detection limit, but this brighter limit effectively takes into account the known drop in detection completeness for J=19.7–20.2 (Irwin priv. comm.). Unlike the Deacon & Hambly (2006) simulations we set no limit on the H-band detection, since objects not detected in the H-band will still be identified as part of our YJ selection. Also, note that the Deacon & Hambly (2006) simulations used a normalisation value of 0.0055 objects per cubic parsec in the mass range 0.1-0.09$M_\odot$ taken from Burgasser (2004). Here we use a normalisation value of 0.0038±0.0013 per cubic parsec calculated by Deacon, Nelemans and Hambly (2008). The results of these simulations are shown in Table 8, where the simulated late T dwarfs were defined as having $T_{\mathrm{eff}} < 1300K$. Mass function power-law indices α and x are also indicated, where the simulations assume functions of the form $dn/dm \propto \mathrm{m}^{-\alpha}$ or $dn/d(\log m) \propto \mathrm{m}^{-x}$ (following Chabrier 2005).

When comparing the observed number of T4-T8.5 dwarfs (from Table 7) to the predicted numbers in Tables 8, and allowing for the associated uncertainties, it is clear that it is not possible to place a significant constraint on the birthrate. However, this comparison favours a range of α between -0.5 and -1.0. Statistically our T dwarf numbers are also reasonably consistent (to within 1.5σ) with α = 0.0. However, they are inconsistent with α of 0.5 and 1.0 at the 2.0 and 2.5σ level respectively. This result is reasonably consistent with the finding of Metchev et al. (2008), who performed a combined 2MASS and SDSS T dwarf search and

Table 8. Simulated late T dwarf (defined as those with T_{eff} <1300K) numbers for LAS DR2 (see text), for which we assumed input forms for the initial mass function of $dn/dm \propto m^{-\alpha}$ or $dn/d(\log m) \propto m^{-x}$, and for the birth-rate of $b(t) \propto e^{-\beta t}$.

Constant birthrate		
$\alpha = -1.0$	$x = -2.0$	15±5
$\alpha = -0.5$	$x = -1.5$	25±9
$\alpha = 0.0$	$x = -1.0$	44±15
$\alpha = 0.5$	$x = -0.5$	57±19
$\alpha = 1.0$	$x = 0.0$	119±40
IMF with $\alpha = 0.0$ or $x = -1.0$		
$\beta = -0.1$		54±18
$\beta = 0.0$		44±15
$\beta = 0.1$		33±11
$\beta = 0.2$		35±12
$\beta = 1.0$		31±11

derived a T dwarf space density that was most consistent with $\alpha = 0.0$ (although based on lower number statistics than here). However, L dwarf mass function constraints suggest higher values of α in the 1-1.5 range (Reid et al. 1999; Cruz et al. 2007). The sub-stellar mass function of young open clusters are generally consistent with $\alpha \simeq 0.5$. However, a lognormal function also offers a reasonable fit to observation (see the Pleiades mass function in figure 4 of Chabrier 2005). The slope of the lognormal mass function gets steeper as one decreases brown dwarf mass, and for $\sim$0.04$M_\odot$ the lognormal mass function slope is consistent with an $\alpha = 0.0$ power law. A detailed comparison between mass function constraints from L and T dwarfs is beyond the scope of this paper, however, it may be that differences occur due to the T dwarfs probing a somewhat lower mass range than the L dwarfs. This would suggest that a single power-law exponent is not optimal when describing the substellar mass function in the field. Clearly a greatly improved picture of the mass function will emerge from the LAS as the survey area grows.

7 CONCLUSIONS AND FUTURE WORK

We have discussed our database selection methods and the photometric follow-up that we performed to search for late T dwarfs and even cooler T_{eff}=400–700K objects in the UKIDSS LAS. These techniques have allowed us to make essentially complete follow-up of our candidates from DR1 and DR2 down to J=19. We have also followed up some candidates from DR3 and a fraction of our fainter candidates from DR1 and DR2 (to J=19.5). Using a variety of spectroscopic facilities we have measured the spectra of our best candidates, and have spectroscopically confirmed 15 new T dwarfs, bringing the total of number of confirmed LAS T dwarf discoveries to 28.

Compared to typical T dwarf properties, one of our new T dwarfs may be metal-poor, two may have relatively low surface gravity, one may have higher than normal surface gravity, and one may be metal rich or have low surface gravity. These assessments are based on comparisons between the spectral morphology and colours of the T dwarfs with

Table 7. T dwarf sample statistics.

Spectral type range	No. in our $J < 19$ DR2 sky (280 sq degs)	Correction to include T dwarfs with $J - H > 0.1$	Final DR2 corrected number to J=19 [a]
T0–T8.5	22–24	+95±27%	35±9
T2.5–T8.5	22–24	+40±15%	24±6
T4–T8.5	19–21	<10%	17±4

[a]Numbers corrected to account for redder ($J - H > 0.1$) T dwarfs outside our selection, LAS photometric uncertainties, unresolved binarity for a binary fraction in the 10–50% range, spatial incompleteness and Malmquist bias (see text).

theoretical models trends, and are thus somewhat speculative. However, all indications are that T dwarf spectra are quite sensitive to their physical properties, and it seems clear that a better understanding of these variations would have important implications for our ability to model T dwarf atmospheres, and potentially constrain (via spectroscopy) the mass, age and composition of T dwarf populations in the field (e.g. Pinfield et al. 2006). To this end, it would be very beneficial to identify T dwarfs whose properties could be constrained without the need to study their spectra. Both T dwarfs and L dwarfs of this type may be found in widely separated binary systems (e.g. Gizis et al. 2001; Wilson et al. 2001; Pinfield et al. 2006; Scholz et al. 2003; Burgasser et al. 2000; Luhman et al. 2007) for which the primary object can be used to constrain system age and composition. Gl570D and HD3651B (Burgasser 2000 and Luhman et al. 2007) are good examples, being analysed for age and abundance by Geballe et al. (2001), Burgasser (2007) and Liu Leggett & Chiu (2007).

The large volume (and large number of T dwarfs) probed by the LAS should yield many T dwarfs in such binary systems, and in this context we made a basic search for possible companions to all confirmed LAS T dwarfs out to a separation of ~10,000AU (at the estimated distances in Table 5), by querying the Simbad astronomical database (operated at CDS). We searched for neighboring objects with either a measured spectral type, a parallax, or a high proper motion, for which we could obtain distance constraints from either parallax or from spectral type and photometry. These distance constraints allowed us to rule out (as possible companions) all the neighboring objects, by comparison with the distance constraints of the T dwarfs. However, proper motion measurements for all LAS T dwarfs would facilitate a more general search for common proper motion companions as the number of LAS T dwarfs grows, which could include white dwarf companions that can yield useful age constraints (e.g. Day-Jones et al. 2008) and are readily identified in SDSS (e.g. Kleinman et al. 2004; Gates et al. 2004; Eisenstein et al. 2006).

The number of blue ($J - H < 0.1$) LAS T dwarfs discovered with our methods shows statistical evidence for a good level of completeness down to $J=19$. This builds on our previous work (e.g. Lodieu et al. 2007) for which a good level of completion was only achieved to $J \sim 18.5$. The increased size of the LAS T dwarf sample allowed us to place some statistical constraints on the sub-stellar mass function.

Indeed, there may be mounting evidence for a steepening (decreasing more rapidly with decreasing mass) sub-stellar mass function in the field, with best-fit α values of ~ 1 and between -1.0 and 0.0 for L and T dwarf populations respectively. In any event, mass function constraints should be greatly improved by larger samples of LAS T dwarfs as the survey continues to grow. In addition, constraints on the brown dwarf birth-rate should be attainable by building on the LAS L and early T dwarf searches mentioned briefly in Section 2.1 (e.g. fig 3 of Deacon & Hambly; fig 10 of Burgasser 2004). For instance, a sample of ~100 L/T dwarfs per $\Delta T_{\rm eff}=100$K range from 1100-1500K (assuming a flat birth-rate) would be capable of ruling out an exponential (e.g. $\tau_g \sim 5$Gyr) birth-rate at a $\sim 5\sigma$ level of significance. An appropriate sample of ~ 400 late L to mid T dwarfs could be identified in the full LAS to $J=18.5$ (for a flat birth-rate).

The discovery of the T8.5 dwarf ULAS J0034-0052 (Warren et al. 2007) in the LAS absolutely demonstrates that UKIDSS is probing unexplored $T_{\rm eff}$ regimes beyond the previously known late T dwarfs. Having said this, parallax and adaptive optics measurements for this and other very late T dwarfs are important if we are to test for unresolved binarity and better constrain luminosity and $T_{\rm eff}$. When comparing the colours of ULAS J0034-0052 with all available LAS T dwarfs, it is possible that a blue trend in $Y - J$ with decreasing $T_{\rm eff}$ may be present. The $J - H$ and $z - J$ colours might also change beyond T8, becoming slightly redder and bluer respectively, although this needs further investigation. These spectral changes would be of great importance not only to our understanding of cool dwarf atmospheres, but also to the potential for finding such objects in the LAS. If it is the case that $T_{\rm eff}=400$-700K objects become bluer in $Y - J$ and redder in $J - H$ than T8 dwarfs, it could be less problematic to identify such candidates to greater $J-$band depth in multi-band searches of the combined LAS and SDSS databases. Indeed, an evolving set of search criteria takes full advantage of the capabilities offered by large general surveys like UKIDSS and SDSS.

REFERENCES

Allen P.R. 2007, ApJ, 668, 492
Allard, F., Hauschildt, P., Alexander, D., Tamanai, A., Schweitzer, A., 2001, ApJ, 556, 357
Allen, P.R., Koerner, D.W., Reid, I.N., Trilling, D.E., 2005, ApJ, 625, 385
Baffa, C. et al., 2001, A&A, 378, 722
Baraffe, I., Chabrier, G., Barman, T.S., Allard, F., Hauschildt, P.H., 2003, A&A, 402, 701
Becklin, E.E., Zuckerman, B., 1988, Nature, 336, 656
Burgasser, A.J. et al. 2000, ApJ, 531, L57
Burgasser, A.J., Kirkpatrick, J.D., Reid, I.N., Brown, M.E., Miskey, C.L., Gizis, J.E., 2003, ApJ, 586, 512
Burgasser, A.J., 2004, ApJS, 155, 191
Burgasser, A.J., McElwain, M.W., Kirkpatrick, J.D., Cruz, K.L., Tinney, C.G., Reid, I.N., 2004, AJ, 127, 2856
Burgasser, A.J. et al., 2002, ApJ, 564, 421
Burgasser, A.J. et al., 2006a, ApJS, 166, 585
Burgasser, A.J., Burrows, A.J., Kirkpatrick, J.D., 2006, ApJ, 639, 1095
Burgasser, A.J., Geballe, T.R., Leggett, S.K., Kirkpatrick, J.D., Golimowski, D.A., 2006b, ApJ, 637, 1067
Burgasser, A.J., Kirkpatrick, J.D., Reid, I.N., Brown, M.E., Miskey, C.L., Gizis, J.E., 2003, ApJ, 586, 512
Burrows, A., Marley, M.S., Sharpe, C.M., 2000, ApJ, 531, 438
Burrows, A., Sudarsky, D., Hubeny, I., 2006, ApJ, 640, 1063
Burrows, A., Sudarsky, D., Lunine, J.I., 2003, ApJ, 596, 587
Carpenter, J.M., 2001, AJ, 121, 2851
Casali, M. et al., 2007, A& A, 467, 777
Casewell, S.L., Dobbie, P.D., Hodgkin, S.T., Moraux, E., Jameson, R.F., Hambly, N.C., Irwin, J., Lodieu, N., 2007, MNRAS, 378, 1131
Chabrier, G., 2003, PASP, 115, 763
Chiu, K. et al., 2006, AJ, 131, 2722
Chiu, K. et al., 2007, arXiv:0712.1229
Cruz, K.L. et al., 2007, AJ, 133, 439
Day-Jones, A.C. et al., 2008, MNRAS, submitted
Deacon, N.R., Hambly, N.C., 2006, MNRAS, 371, 1722
Deacon, N.R., Nelemans, G., Hambly, N.C., arXiv0804.2455
Dye, S. et al., 2006, MNRAS, 372, 1227
Elias, J.H., Joyce, R.R., Liang, M., Muller, G.P., Hilman, E.A., George, J.R., 2006, in Ground-based and Airborne Instrumentation for Astronomy, eds, McLean, I.S., Iye, M., Proceedings of SPIE, 6269, 138
Eisenstein D.J., et al., 2006, ApJS, 167, 40
Epchtein, N. et al. 1997, Msngr, 87, 27
Gates, E. et al., 2004, ApJ, 612, L129
Geballe, T.R., Saumon, D., Leggett, S.K., Knapp, G.R., Marley, M.S., Lodders, K., 2001, ApJ, 556, 373
Geballe, T.R. et al., 2002, ApJ, 564, 466
Gizis, J.E., Kirkpatrick, J.D., Burgasser, A.J., Reid, I.N., Monet, D.G., Liebert, J., Wilson, J.C., 2001, ApJ, 551, L163
Golimowski, D.A. et al., 2004, AJ, 127, 3516
Hambly, N.C., et al., MNRAS, in press, arXiv:astro-ph/0711.3593
Hauschildt, P.H., Baron, E., 1999, Journal of Computational and Applied Mathematics, 102, 41
Hewett, P., Warren, S.J., Leggett, S.K., Hodgkin, S.T., 2006, MNRAS, 367, 454
Hodapp, K.W. et al., 2003, PASP, 115, 1388

Irwin, M.J., et al., 2004, Proceedings of the SPIE, 5493, 411

Kendall, T.R. et al., 2007, A&A, 466, 1059

Kirkpatrick, J.D., Henry, T.J., Liebert, J., 1993, ApJ, 406, 701

Kirkpatrick, J.D. et al., 1999, ApJ, 519, 802

Kirkpatrick, J.D. et al., 2000, AJ, 120, 447

Kirkpatrick, J.D., 2005, ARA&A, 43, 195

Kleinman, S.J. et al., 2004, ApJ, 607, 426

Knapp, G. R. et al., 2004, AJ, 127, 3553

Knutson, H.A. et al., 2007, Nature, 447, 183

Kobayashi, N. et al., 2000, Proc.SPIE 4008: Optical and IR Telescope Instrumentation and Detectors, eds M Iye & A. F. Moorwood, 1056

Kucinskas, A. et al., 2005, A&A, 442, 281

Kucinskas, A. et al., 2006, A&A, 452, 1021

Lawrence, A. et al., 2007, MNRAS, 370, 1599

Leggett, S.K. et al., 2006, MNRAS, 373, 781

Leggett, S.K. et al., 2007, ApJ, 667, 537

Liu, M.C., Leggett, S.K., Chiu, K., 2007, ApJ, 660, 1507

Liu, M.C. et al., 2006, ApJ, 647, 1393

Lodieu, N. et al., 2007a, MNRAS, 379, 1423

Lodieu, N., Dobbie, P.D., Deacon, N.R., Hodgkin, S.T., Hambly, N.C., Jameson, R.F., 2007b, MNRAS, 380, 712

Luhman, K. et al., 2007, ApJ, 654, 570

Marley, M.S., 2007, AAS, 210, 9604

Marley, M.S., Seager, S., Saumon, D., Lodders, K., Ackerman, A.S., Freedman, R.S., Fan, X., 2002, ApJ, 568, 335

Masana, E., Jordi, C., Ribas, I., 2006, A&A, 450, 735

Metchev, S.A., Kirkpatrick, J.D., Berriman, G.B., Looper, D., 2008, ApJ, 676, 1281

Nakajima, T., Oppenheimer, B.R., Kulkarni, S.R., Golimowski, D.A., Matthews, K., Durrance, S.T., 1995, Nat, 378, 463

Pinfield, D.J. et al., 2006, MNRAS, 368, 1281

Pinfield, D.J., Dobbie, P.D., Jameson, R.F., Steele, I.A., Jones, H.R.A., Katsiyannis, A.C., 2003, MNRAS, 342, 1241

Ramsay Howat, S.K. et al., 2004, in Ground-based Instrumentation for Astronomy, Proceedings of the SPIE, 5492, 1160

Reid, I.N. et al., 1999, ApJ, 521, 613

Reid, I.N., Lewitus, E., Allen, P.R., Cruz, K.L., Burgasser, A.J., 2006, AJ, 132, 891

Roche, P.F. et al., 2003, in Instrument Design and Performance for Optical/Infrared Ground-based Telescopes, Proceedings of SPIE, eds Iye M., Moorwood A.F.M., 4841, 901

Saumon, D. Marley, M.S., Lodders, K., Freeman, R.S., 2003, in Brown Dwarfs, Proceedings of IAU Symposium 211, eds Eduardo Martin, ASP Series, 345

Saumon, D. et al., 2007, ApJ, 656, 1136

Saumon, D., Marley, M.S., Cushing, M.C., Leggett, S.K., Roellig, T.L., Lodders, K., Freedman, R.S., 2006, ApJ, 647, 552

Skrutskie, M.F. et al., 2006, AJ, 131, 1163

Scholz, R.D., McCaughrean, M.J., Lodieu, N., Kuhlbrodt, B., 2003, A&A, 398, L29

Tokunaga, A.T., Simons, D.A., Vacca, W.D., 2002, PASP, 114, 180

Tsuji, T., Nakajima, T., Tanagisawa, K., 2004, ApJ, 607, 511

Warren, S.J., Hewett, P., 2002, ASPC, 283, 369

Warren, S.J. et al., 2007a, MNRAS, 381, 1400

Warren, S.J. et al., 2007b, MNRAS, 375, 213

Warren, S.J. et al., 2007c, arXiv:astro-ph/0703037

Wilson, J.C., Kirkpatrick, J.D., Gizis, J.E., Skrutskie, M.F., Monet, D.G., Houck, J.R., 2001, AJ, 122, 1989

York, D.G., et al., 2000, AJ, 120, 1579

Zapatero-Osorio, M.R. et al., 2008, A&A, 477, 895

This paper has been typeset from a TeX/ LaTeX file prepared by the author.